Advances in Colloid and Interface Science 171–172 (2012) 36–52

Contents lists available at SciVerse ScienceDirect

Advances in Colloid and Interface Science

journal homepage: www.elsevier.com/locate/cis

Casein micelles and their internal structure

Cornelis G. de Kruif [a,b,*], Thom Huppertz [a], Volker S. Urban [c], Andrei V. Petukhov [b]

[a] NIZO food research, PO Box 20, 6710 BA, Ede, The Netherlands
[b] Van 't Hoff laboratory for Physical and Colloid Chemistry, Utrecht University, Padualaan 8, 3584 CH Utrecht, The Netherlands
[c] Center for Structural Molecular Biology, Oak Ridge National Laboratory, Oak Ridge, Tennessee 37831, USA

ARTICLE INFO

Available online 20 January 2012

Keywords:
Casein micelle
Structure
Nanocluster model
SANS
Model calculations

ABSTRACT

The internal structure of casein micelles was studied by calculating the small-angle neutron and X-ray scattering and static light scattering spectrum (SANS, SAXS, SLS) as a function of the scattering contrast and composition. We predicted experimental SANS, SAXS, SLS spectra self consistently using independently determined parameters for composition size, polydispersity, density and voluminosity. The internal structure of the casein micelles, i.e. how the various components are distributed within the casein micelle, was modeled according to three different models advocated in the literature; i.e. the classical sub-micelle model, the nanocluster model and the dual binding model. In this paper we present the essential features of these models and combine new and old experimental SANS, SAXS, SLS and DLS scattering data with new calculations that predict the spectra. Further evidence on micellar substructure was obtained by internally cross linking the casein micelles using transglutaminase, which led to casein nanogel particles. In contrast to native casein micelles, the nanogel particles were stable in 6 M urea and after sequestering the calcium using trisodium citrate. The changed scattering properties were again predicted self consistently.

An important result is that the radius of gyration is independent of contrast, indicating that the mass distribution within a casein micelle is homogeneous. Experimental contrast is predicted quite well leading to a match point at a D_2O volume fraction of 0.41 ratio in SANS. Using SANS and SAXS model calculations it is concluded that only the nanocluster model is capable of accounting for the experimental scattering contrast variation data. All features and trends are predicted self consistently, among which the 'famous' shoulder at a wave vector value $Q = 0.35\ nm^{-1}$

In the nanocluster model, the casein micelle is considered as a (homogeneous) matrix of caseins in which the colloidal calcium phosphate (CCP) nanoclusters are dispersed as very small (about 2 nm) "cherry stones" at an average distance of 18.6 nm. Attached to the surface of the nanoclusters are the centers of phosphorylation (3-5 nearby phosphorylated amino acid residues) of the caseins. The tails of the caseins, much larger than the CCP clusters, then associate to form a protein matrix, which can be viewed as polymer mesh with density fluctuations at the 2 nm scale. The association of the tails is driven by a collection of *weak interactions*. We explicitly use *weak interactions* as a collective term for hydrophobic interactions, hydrogen bonding, ion bonding, weak electrostatic Van der Waals attraction and other factors (but not the strong calcium phosphate interaction) leading to self association. The association is highly cooperative and originates in the weak interactions. It is the cooperativety that leads to a stable casein micelle. Invariably, κ-casein is thought to limit the process of self association leading to stabilization of the native casein micelle.

Contents

* Corresponding author at: NIZO food research, PO Box 20, 6710 BA, Ede, The Netherlands. Tel.: +31 318 659511; fax: +31 318 650400.
E-mail address: kees.dekruif@nizo.nl (C.G. de Kruif).

0001-8686/$ – see front matter © 2012 Elsevier B.V. All rights reserved.
doi:10.1016/j.cis.2012.01.002

1. Introduction

Milk contains colloidal particles that are composed of a complex of associated protein and calcium phosphate. These heterogeneous association colloids are named casein micelles [1]. Notwithstanding their abundance and countless number of studies, there is still not a unified picture of their structure and properties. In particular concerning their size (distribution) and their internal structure literature is at best unclear. In a recent book on Biopolymers, Semenova and Dickinson said: *The structure of the naturally created casein particle, the ´casein micelle´, has been the subject of investigation (and controversy) for the best part of a century* [2]. In a recent interesting SAXS study on casein micelles from Cabanes group the authors say: *Yet their structure is still a puzzle and is continuously the subject of furious debates among the scientific community* [3].

Here we aim to not intensify the debate but to present new scientific facts that contribute to unraveling the internal structure of the casein micelle and to contribute to a better understanding of its properties. The importance of casein micelles can hardly be overestimated in view of their tremendous economical and nutritional value.[1]

From a product technological and dairy industry point of view the caseins are by far the most important and valuable component of milk. The main dairy products as liquid milk, cheese and yoghurt derive their textural, sensory and nutritional properties from the caseins. Replacing caseins by plant proteins leads to products with different textural and sensorial quality.

The protein fraction of the casein micelles, which represents ~93% of its dry mass, is composed of four individual gene product components, denoted α_{s1}-, α_{s2}-, β- and κ-casein, which differ in primary structure and type and degree of post-translational modification [4]. The remainder of the micellar solids consists of inorganic material, collectively referred to as colloidal calcium phosphate (CCP) or micellar calcium phosphate (MCP). Over the last 50 years there have been reviews on the casein micelles at regular intervals [5-20]. Recently the structure of casein micelles was discussed from a structural biology point of view [16] suggesting that protein-protein interactions is leading according to the structural biology tenet that structure follows function. However no reference was made to a detailed study of the mammary glands by Neville [17] who gives a detailed account of the transport of Ca in the Golgi apparatus and suggests that calcium concentration is the determining factor rather than the protein, which is in line with the views of Smyth et al. [18].

Thus, although the casein micelles are essential for the neonate and are at the heart of the dairy industry, it is remarkable that there is still quite some confusion, if not myths, around these particles in milk. Notwithstanding all these research and review papers, there is no uniform picture of what a casein micelle is, how it is formed, what its structure is and how it behaves. This fact is recognized and often emphasized in publications concerning casein micelles.

In this paper we will analyze and review existing and new data on the casein micelles and aim to present a self-consistent picture based on quantitative data, rather than on electron microscopy pictures. For this we will use (dynamic) light scattering, SANS and SAXS data. We will translate the consequences of proposed sub-structures of casein micelles into calculated scattering spectra and confront that with experiment. Most importantly we will conserve mass, i.e. we will maintain the condition that the total mass of a casein micelle is given by density times volume and that the ratio of the various components is according to the overall composition of casein micelles.

In previously-published SANS studies [21-24], the spectra obtained are very similar, if not identical. They agree on a (faint) shoulder at $Q \approx 0.35\ nm^{-1}$, especially at low contrast, which was attributed to sub-micellar structures on a length scale of 18 - 20 nm. In SAXS studies [25-30] the obtained spectra are very similar and show a shoulder at $Q \approx 1\ nm^{-1}$. In a Kratky plot, two distinct maxima are present. We also measured SAXS spectra which are again very similar. So there is a broad agreement on the shape and characteristics of the SANS/SAXS spectra which all show a decaying function with three ´plateaus´ or ´shoulders´. Invariably, the first one at low Q is attributed to the form factor of the casein micelles. The intermediate shoulder, at about $0.35\ nm^{-1}$, is not present in all SAXS spectra but particularly in SANS spectra. Gebhardt [29] varied calcium concentration in their μGISAXS spectra and attributed this shoulder to the form factor of sub-micellar particles ranging in diameter between 10 and 20 nm. Finally there is a shoulder at about $Q \approx 1\ nm^{-1}$or somewhat larger wave vector which corresponds to a particle size (characteristic length) of a few nanometers.

Based on this, the casein micelle was considered a hierarchical structure of sub structures. Data analysis was based on summing the form factors of the different substructures with adjustable sizes and amplitudes. This procedure was also followed by Hansen [24] and formalized by Beaucage [31] in a unified spectrum of exponentially decaying and power law decaying functions for each substructure, requiring an amplitude, a radius of gyration, and a power law exponent. Thus each substructure requires at least three adjustable parameters. For a casein micelle therefore a minimum of 6 parameters is required. If more details, e.g. a third shoulder, are introduced three more adjustable parameters are required. Of course the spectra can be well fitted with this number of adjustable parameters. Question however is what do the numbers mean and, more importantly, dimension should not change with contrast.

[1] The world production of milk is about 6.10^{11} liters per annum, (cow 85% and buffalo 11%, from FAO). The world population is estimated at 6.9 10^9 (U.S. Census Bureau) In other words the milk production is 250 ml (a soda bottle) per person per day! If 1% of the world population is lactating the world production of human milk is about 6.6 10^7 *365* 0.6liter = 1.2 10^10liter per year or 2% of the animal milk. The world population is growing with 1.4% per annum and milk production by 1% per annum over the last 25 years.

In this paper we will analyze and review existing and new SANS and SAXS data. The difference with previous studies is that we will introduce a new way of analyzing the data, but more importantly our calculations are basic predictions, free of main adjustable parameters such as amplitudes and casein micelle size. In doing so we were able to describe light, SAXS and SANS spectra with the same set of parameters. The parameters are based on independent measurements of size, density, composition of the casein micelles. The aim is to get a better insight into the internal structure of casein micelles.

2. Theoretical background

2.1. Small angle neutron scattering (SANS)

First we outline the general principles and the underlying equations, in some detail, of small angle neutron scattering (SANS) and then after analyzing the possible sub-structure we will present the pertinent equations. Actually these equations apply to small angle X-ray and light scattering mutatis mutandis.

The normalized intensity of neutrons (light , X-rays) scattered by a colloidal dispersion is given by [32-34]:

$$I(Q) = \left(\rho_p - \rho_{solv}\right)^2 N_p V_p^2 P(Q) S(Q) \quad (1)$$

Below we will discuss the respective terms in Eq. (1), which have the usual meaning as applied in scattering experiments. Q is the scattering wave vector [m^{-1}]. In SANS the scattering angle θ is small. Typically a 1 meter diameter detector is placed at a distance of 10 meters from the sample and the wavelength of the cold neutrons used is typically 1 nm. Thus, Q varies approximately between 0 and 1 nm^{-1}. The symbols ρ_p and ρ_s denote the scattering length densities (SLD) of the particles and solvent respectively. In SAXS electron density is used. SLD can be calculated from mass density, the atomic scattering length and the atomic composition as:

$$\rho = \frac{d_m N_{Av}}{M} \sum_i n_i b_i \quad (2)$$

in which d_m is the mass density [kg/m^3], N_{Av} =6.022*10^{23} , M is the atomic mass and n_i is the number of atoms *i* with a scattering length b_i. Table 1 lists the scattering length of common atoms in casein micelles. In neutron scattering the property of interest is the coherent scattering length b_{coh}, while the incoherent scattering length b_{inc} contributes to a background signal and b_{abs} is the absorption length.

The coherent scattering length density of water is ρ_{H2O} = -0.56172 10^{14} m^{-2} = -0.56172 10^{10} cm^{-2}. The scattering length density of deuterated water is ρ_{D2O} = 6.405110^{10} cm^{-2}.We will express all scattering length densities in 10^{10} cm^{-2} units, which is a length per volume.

Table 1
Neutron scattering lengths of some elements.

Nucleus	$b_{coh}/10^{-5}$ Å	$b_{inc}/10^{-5}$ Å	$b_{abs}/10^{-5}$ Å
^{1}H	-3.741	25.3	1.5
^{2}D	6.671	4.1	0
^{12}C	6.646	6.7	0.0
^{16}O	5.803	5.8	0.0
^{14}N	9.362		
^{32}S	2.847		
^{40}Ca	4.78		
^{31}P	5.13		
CH_3	-4.577		

Contrast is the difference in SLD between particle and solvent (or environment) and thus depends on the volume fraction Φ of D_2O in the solvent

$$\Delta\rho(\Phi) = \rho_p(\Phi) - \rho_{solv}(\Phi)$$

Since part of the protons may be exchanged if casein micelles are dispersed in D_2O the scattering length density depends on the solvent composition, i.e., the volume fraction Φ as well. These scattering lengths were calculated from the known primary structure of the proteins and their concentration in milk. The scattering length densities as used in further calculations are listed below.

Scattering length density of solvent

$$\rho_{solv}(\Phi) = (-0.56172(1-\Phi) + 6.4051\Phi)10^{10} cm^{-2}$$

The SLD of a casein micelle is calculated from the contribution of the caseins proteins, the solvent fraction in the particle and the CCP.

Scattering length density of casein protein in casein micelles (not including the CCP)

$$\rho_{prot}(\Phi) = ((1-\Phi)1.72 + \Phi 3.12)10^{10} cm^{-2}$$

The SLD at Φ = 0 is 1.72 10^{10} cm^{-2} and is calculated using the atomic composition of the caseins. With this expression for the SLD of the protein matrix the match point is found at Φ = 0.41 as it is experimentally found.

The scattering length density of CCP in the casein micelles can be calculated unambiguously if the composition, water content and density is known. For instance assuming the CCP consists of calcium phosphate $CaHPO_4.2H_20$ with a density of 2.31 kg/L we find:

$$\rho_{CaP}(\Phi) = ((1-\Phi)3.82 + \Phi 6.2)10^{10} cm^{-2}$$

Assuming CCP consists of hydroxy apetite, $Ca_{10}(PO_4)_6(OH)_2$

$$\rho_{HAP}(\Phi) = ((1-\Phi)3.07 + \Phi 3.36)10^{10} cm^{-2}$$

However the precise values depend very much on the assumed density of the CCP. Holt [35] assumed a crystalline structure for his calcium phosphate precipitates at neutral pH . But there are reasons to assume a more amorphous structure due to the presence of citrates [17] and the presence of the phospho-peptide chains. All of this will lower the SLD of the CCP. Actually, it is to be remarked that scattering intensity at zero angle is independent of the density or volume of the particles. Contrast is inversely proportional to volume while scattering scales in volume squared. Whatever the precise value of the CCP may be, it is safe to say that it will be close to the protein in H_2O. In other words secondary features due to the CCP will be masked in H_2O.

In order to calculate the average scattering length density of a casein micelle particle we have to integrate the scattering length density over the volume of the particle. We then assume that the particles are homogeneous and we account for the colloidal calcium phosphate as the excess over the casein protein.

$$\rho_p(\Phi) = \frac{\int_0^{R_0} 4\pi \frac{\rho_{prot}(\Phi)}{4.4} r^2 dr + \frac{N_{nc}}{N_{cm}} \int_0^{R_{nc}} 4\pi \left(\rho_{nc}(\Phi) - \frac{\rho_{prot}(\Phi)}{4.4}\right) r^2 dr}{\int_0^{R_0} \frac{4\pi r^2}{4.4} dr} \quad (3)$$

where N_{cm} and N_{nc} represent the total number of casein micelles and nanoclusters respectively. Therefore N_{nc}/N_{cm} = number of nanoclusters per micelle particle ≈ 300. The number of nanoclusters may increase tenfold if the CCP is distributed differently, but the total

mass must be constant and therefore mean contrast does not change. Scattering does change of course.

If the distribution $\rho_{prot}(\Phi)$ and $\rho_{nc}(\Phi)$ is homogeneous then:

$$\rho_p(\Phi) = \frac{\frac{\rho_{prot}(\Phi)}{4.4}\frac{4}{3}\pi R_0^3 + \frac{N_{nc}}{N_{cm}}\left(\rho_{nc}(\Phi) - \frac{\rho_{prot}(\Phi)}{4.4}\right)\frac{4}{3}\pi R_{nc}^3}{\frac{4}{3}\pi R_0^3/4.4} \tag{4}$$

The factor 1/4.4 in the SLD of the casein matrix is due to the fact that only a fraction 1/4.4 of a casein micelles is made up of protein, or voluminosity is 4.4 $cm^3\ g^{-1}$ protein [21, 36, 37]. The SLD of the casein matrix is calculated from the known amino acid composition of the caseins. The exchangeability of protons can be estimated from dissociation constants, but remains difficult to estimate exactly. We set the number of exchangeable protons such that the calculated match point of the casein micelle particles is 41% D_2O as follows from experiment.

Fig. 1 illustrates how the SLD varies as a function of volume fraction D_2O. The point where the SLD of the solvent intersects the SLD of the particle is called the match point and contrast is equal to zero ($\Phi = 0.41$) and determined experimentally to be between Φ is 0.39 and 0.44 [21-24].

The term N_p in Eq. (1) is the number density of particles, whereas the term V_p in Eq. (1) is the molar volume of the dispersed particles. V_p must be a Z-average, but here we integrate (numerically) over the size distribution. The next term in Eq. (1) is $P(Q)$ which is called the scattering form factor and accounts for interference of scattered electromagnetic wave or neutrons from within a single particle. $P(Q)$ can be calculated from the amplitude of the Fourier transform of scattering length density within a particle.

$$B_{cmp}(Q, r_i, \Phi) = \int_0^{r_i} 4\pi\left(\left(\frac{1}{4.4}\rho_p(r,\Phi) + \frac{3.4}{4.4}\rho_{solv}(\Phi)\right) - \rho_{solv}(\Phi)\right) r^2 \frac{\sin(Qr)}{(Qr)} dr \tag{5}$$

If the particles are homogeneous it reduces to

$$B_{cmp}(Q, r_i, \Phi) = \rho_p(\Phi) \int_0^{r_i} 4\pi r^2 \frac{\sin(Qr)}{(Qr)} dr \tag{6}$$

Usually the scattering is normalized on the scattering at Q = 0

$$B_{cmp}(0, r_i, \Phi) = \int_0^{r_i} 4\pi\left(\left(\frac{1}{4.4}\rho_p(r,\Phi) + \frac{3.4}{4.4}\rho_{solv}(\Phi)\right) - \rho_{solv}(\Phi)\right) r^2 dr$$

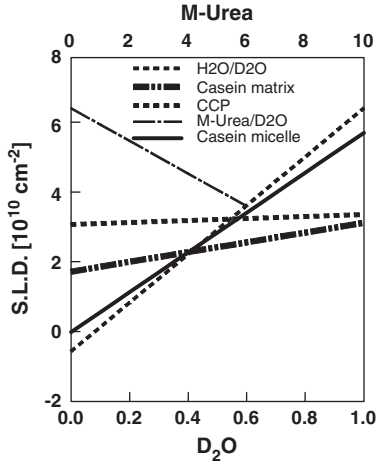

Fig. 1. The variation of the scattering length density of the protein, the colloidal calcium phosphate, the casein micelle particle and finally the contrast as a function of volume fraction of D_2O On adding 6 M Urea to D_2O contrast is lowered to 4 $.10^{10}$ cm^{-2}.

The normalized form factor is then calculated as

$$P_{cmp}(Q, r_i, \Phi) = \frac{B_{cmp}(Q, r_i, \Phi)^2}{B_{cmp}(0, r_i, \Phi)^2} \tag{7}$$

For a homogeneous sphere with r = R, $P_{cmp}(Q, r_i)$ is given by Eq. (8) and does not depend on contrast anymore.

$$P(Q, R) = \left(\frac{(QR)\cos(QR) - \sin(QR)}{(QR)^3}.3\right)^2 \tag{8}$$

Since the casein micelles are not monodisperse in radius R we used a ln-normal size distribution [12, 38] In addition, we recently made extensive dynamic light scattering experiments. A polydisperse form factor is than given by:

$$PI_{cmpol}(Q) = \frac{\int_0^{\max} p(Q, r_i).F_{\ln}(r_i)\left(\frac{4}{3}\pi r_i^3\right)^2 dr_i}{\int_0^{\max} .F_{\ln}(r_i) dr_i} \tag{9}$$

Where $F_{\ln}(r)$ is the ln-normal size distribution, (see Eq. (10)).

The challenge here is to model the mass and scattering distribution within the micelle in order to perform the integration in Eq. (9). This will be discussed in the following section.

The ln-normal size distribution is given by:

$$F_{\ln}(r) = \frac{1}{\left(r\beta\sqrt{2\pi}\right)} \exp\left[-\left(\frac{\ln\left(\frac{r}{R_{10}}\right)}{\beta\sqrt{2}}\right)^2\right] \tag{10}$$

The median value of the distribution is $R_{10} = 55$ nm, and the width of the distribution is determined by $\beta = 0.27$. Note that these numbers are given for illustration purposes here, but actually correspond to experimental results as presented below. In Fig. 2 a representation is given of the size distribution in particle radius (as given by Eq. (10)), against r in nm. The dashed line is a Gaussian distribution. The width follows from: $\beta \approx \sqrt{\ln(\sigma_{std}^2 + 1)}$. In dynamic light scattering, the polydispersity in scattering leads to an apparent measured hydrodynamic radius of 75 nm at 90 degrees scattering, using a green laser and a cumulant analysis. Pooled milk has larger micelles and a somewhat higher polydispersity and apparent DLS-size is found to be 100 nm and higher.

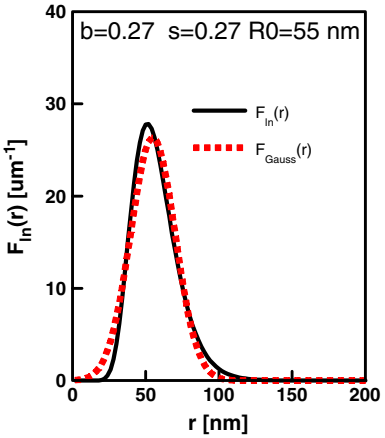

Fig. 2. Particle size frequency, in a ln-normal and Gaussian distribution. $R_0 = 55$ nm, $\beta = 0.27$, $\sigma = 0.27$.

The last term in Eq. (1) is called the structure factor S(Q). This term accounts for the intra-particle interference and becomes important for non-dilute or strongly-interacting particles.

The separation of the inter-particle interference from the intra-particle interference is called the decoupling approximation and is only allowed for reasonably mono-disperse systems. Here, we will take the structure factor of the casein micelles as 1 for all Q and therefore use Eq. (9). This may only introduce an error for the very small Q values where experimental data are usually less reliable due to the presence of small aggregates. The value of the structure factor can be calculated from statistical mechanics theory [39, 40]. We will use S(Q) of excluded volume particles to modulate the intra particle scattering of the micelles, due to the (assumed) presence of CCP as small (nano or Angstrom sized) clusters. The size and distribution of the CCP is to be determined.

3. Structure of casein micelles

3.1. How to shape a casein micelle particle?

Bovine casein micelles contain about 7% CCP on a dry matter basis. Neutron scattering spectra show no secondary structure in H_2O, where it is a smoothly decaying scattering function [23]. Secondary structure at $Q \approx 0.35\ nm^{-1}$ is most pronounced near the overall match point of the casein micelle particles (41% D_2O) and corresponds to a correlation length of 18.6 nm in real space [21-24]. Small angle X-ray scattering experiments show a (faint) shoulder in the scattering spectra at $Q \approx 1\ nm^{-1}$[25-28]. Pignon [26] and Shukla [30] conclude that their detailed and extensive electron microscopy and SAXS data suggest that the nanocluster model is consistent with their data. Looking at Fig. 1, we see that the difference in SLD of the protein and the CCP is smallest in H_2O. In other words, from a scattering point of view the casein particles are most homogeneous in H_2O, at any given distribution of matter.

This leads to an important conclusion: if the secondary features (around $Q \approx 0.35\ nm^{-1}$) were due to in-homogeneities in protein distribution, the secondary features would be most visible in H_2O. The same argument would hold a fortiori for x-ray scattering. In SAXS, there is shoulder at $Q \approx 1\ nm^{-1}$ which according to Pignon [26] corresponds to a radius of gyration of 5.4 nm and could be attributed to the CCP nanoclusters. We argue, however, that this shoulder in SAXS can be both due to protein or CCP. In SANS, features as amyloidal β-sheets or even nanotubes would, if present, be visible best in H_2O. However secondary features at $Q \approx 0.35\ nm^{-1}$, become visible near the protein match point and in D_2O rich solvents. Now suppose that the protein was distributed in-homogeneously or that it would contain, as suggested previously, ´empty´ pockets [41] or channel structures [42]. Then, near the match point, these features would disappear like a glass rod in a beaker of toluene. What this means is secondary features in SANS spectra are due to something with a SLD different from the protein and the most likely candidate is the CCP. This argument is corroborated by an experiment in which we added 6 M urea (in D_2O) to completely cross-linked casein nanogels [43]. The addition of 6 M urea lowers the SLD of the solvent to that of the casein protein matrix. Therefore the CCP is seen more prominently. Again, and in conclusion, we observe an increase in secondary features in SANS at $Q \approx 0.35\ nm^{-1}$, which are thus due to the presence of the CCP. The most likely candidate for the shoulder at $Q \approx 1\ nm^{-1}$ is protein in-homogeneity in SAXS measurements, because the scattering amplitude of (very) small CCP clusters (7% w/w) is too small to become visible. Remains the crucial question of how is the CCP distributed in the micelles?

In order to calculate the scattering intensity of casein micelles we need to adopt a distribution of the scattering length density for which there are several options. First we shortly review the existing models and then calculate the scattering spectrum that can be associated with the various models. The oldest model (for review see [19, 41]) was introduced by Waugh [44] (Fig. 3a) and later Schmidt [45] (Fig. 3b) and was amended by Walstra (Fig. 3c) [46, 47]. Horne [15, 48] proposed the dual binding model. The basis of all these models was the observation that caseins self assemble and micellar structures even in the absence of calcium, as they do indeed. The CCP then glues together the protein sub-micelles. It is for these reasons that casein sub-micelles are imagined, which are glued together by the CCP. These ideas were in line with the structural biology tenet that structure follows function. Supposedly, support for the sub-micelle was found in the shoulder in the SANS spectra at $Q \approx 0.35\ nm^{-1}$, leading to a correlation length of about 18.6 nm radius.

In the sub-micelle model and the dual-binding model, the CCP is therefore considered (and modeled in our calculations below) as being located at the periphery of a small sphere (sub micelle) of 9.3 nm radius so as to account for the correlation length observed in SANS spectra of casein micelles. If the sub-micelles were packed in a random close packing manner than there are about 10 nearest neighbors for each sub-micelle [49]. Therefore we assumed 10 CCP clusters per sub micelle and a total of $(R_V/9.3\ nm)^{3}$*10/2 CCP clusters per casein micelle. With a volume average $R_V = 62$ nm the number of gluing clusters would be about 1500. Their volume would be about 1/5 of the nanoclusters and their radius 1.47 nm.

Following these early casein micelle models Pedersen and coworkers [24] calculated the scattering using Eq. (9)) with P(Q) the form factor of a of a large sphere (100 nm) while the internal structure of a casein micelle was represented by a homogeneous sub-micelle (6-9 nm radius) by the form factor of a small sphere. Each casein micelle particle contained a few hundred (fitting parameter) sub-micelles. This approach is allowed if the sub-micelles are much smaller than the casein micelle particle. However in this approach it is not clear what causes the secondary features. Another model used for so-called micro gel particles and micellar structures is a homogeneous sphere with a tailing off due to a less dense corona of polymer molecules. This model was successfully used by Pedersen and Stieger [51] to model polymeric micelles and the swelling of PNIPAM micro gels. Extending the scattering density of the casein micelles with a corona (we tried different assumptions for the tailing off) gave unsatisfactory results. Adding a corona leads to a Q^{-2} drop off of the form factor which is clearly not present in the experimental spectra. We also concluded, in agreement with Pedersen, [24] that a poly-disperse homogeneous sphere correlated best with the experimental spectra.

The more recent model of casein micelles is the nanocluster model of Holt [12, 50] (Fig. 3e). In this nanocluster model, the CCP is dispersed as small 'cherry stones' in a homogeneous protein matrix (a nanogel). The basis of the nanocluster model is the idea that phosphorylated caseins bind to the growing nanoclusters so as to prevent calcification of the mammary gland. The protein tails sticking out of the nanoclusters associate with other proteins through a collection of *weak interactions* to form a more or less homogeneous protein matrix. We explicitly use *weak interactions* as a collective term for hydrophobic interactions, hydrogen bonding, ion bonding, weak electrostatic interactions and other factors (but not the strong calcium phosphate interaction) leading to self association. Just as in the case of pure β-casein and pure κ-casein micelles the association is highly cooperative and originates in the weak interactions [52-54]. Actually the interaction between a pair of β-casein molecules (as suggested in the dual binding model) is unfavorable as follows from the shell model [54]. Only if a larger number of proteins interact simultaneously the interaction becomes thermodynamically favorable. The heterogeneity of the casein proteins could be taken as an indication for heterogeneity of the *weak interactions*. It is the cooperativety or multiplicity of the interactions that leads to a stable casein micelle. Invariably, κ-casein is thought to limit the process of self association leading to stabilization of the native casein micelle.

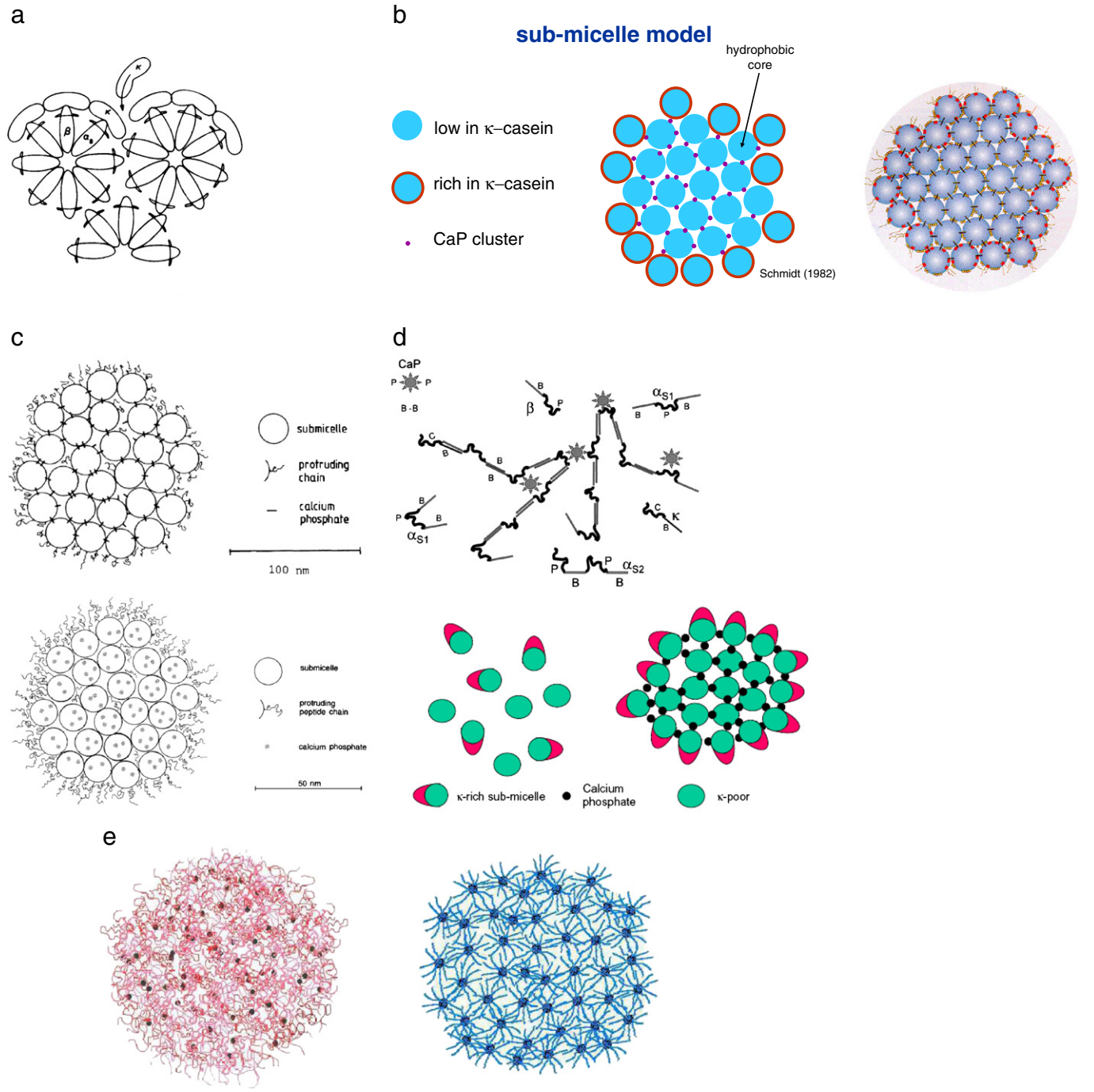

Fig. 3. a. Model of casein micelles proposed by Waugh 1958 [44]. b. Representations of the model of casein micelles proposed by Schmidt [45]. c. Representations of the model of casein micelles proposed by Walstra 1990 [46] and 1999[47]. Note the change in scale and position of the CCP. d. Representation of the dual binding model proposed by Horne 2003 [48], and the interpretation of Schmidt's model in a review 2005 [15]. e. Representations of the model of casein micelles proposed by Holt, [50, 12]. Collection of (artists) impressions of the casein micelle particle.

Detailed specification of the weak interactions as in the dual-binding model is based on imagination rather than thermodynamics.

We assumed that the distribution of the nanoclusters, i.e., the CCP, (size to be determined and specified) could be described by a fluid like distribution in a further homogeneous protein matrix. Hence, we multiplied the excess scattering of the nanoclusters with a structure factor accounting for the distribution of the nanoclusters. We assigned a correlation length of 18.6 nm so as to account for the experimentally observed correlation length. Finally in many artists impressions of casein micelle particles the so-called sub-micelles are surrounded by a layer of CCP. This is from a geometrical point of view very similar to the Waugh/Schmidt/Walstra model (Fig. 3a-c) since the CCP is not found in very small clusters but smeared out. That would also accommodate the fine distribution of CCP as required by the dual binding model [15, 48]. It is mentioned, that Walstra [46] (Fig. 3c.2) later proposed a kind of hybrid sub-micelle model by no longer placing the CCP at the periphery of the sub-micelles but within the sub-micelles. In our calculations, we adopted all three models, but always with the constraint of total mass of protein and CCP in the casein micelles. Actually, in doing so, the earlier models where about ten CCP clusters glues the sub micelles, but also the dual binding model, are ruled out simply because the large number of

Angstrom-sized CCP contribute negligibly to scattering. These conclusions follow from extensive calculations as presented below. The mass of the CCP is 7% w/w of the protein. Decreasing the size of the CCP increases their number, but scattering is proportional to φ^2_{ccp}/n_{ccp}. Volume fraction, φ_{ccp} is (must be about) constant and so if the number increases scattering goes down.

4. Theoretical modeling of the scattering from composite particles

Several approaches have been developed to calculate the scattering of casein micelles. For example, Pedersen and coworkers [24] has elegantly solved the problem by subdividing the micelle in a large number of smaller sub-particles (sub micelles if one wishes) while the medium in between the sub-particles is assumed to have no contrast relative to the solvent. Pignon et al. [26, 27] used a global or universal fitting of the experimental data. Bouchoux [3] used a sponge or cell model in which cells are randomly occupied by either type of component according to the overall volume fraction of each component. It implies that (scattering length) density is an adjustable parameter. Basically all this is a reverse engineering or interpretation of the data giving structural parameters which can be related to proposed models.

We developed a new approach that allows changing internal structure and scattering contrast within the casein micelles and then predict the scattering spectrum. This is a much more challenging approach, because we start off with the known composition and the only freedom is to distribute matter in space. Then, varying contrast as in SANS using D_2O/H_2O mixtures or SAXS we must reproduce all spectra with one distribution of (conserved) mass. We developed the following approach.

Suppose we would have an "infinite" slab of material which is composed of caseins and colloidal calcium phosphate in the exact composition as casein micelles. The material slab is continuous and has the same structure as the interior of the casein micelles. An ultracentrifugal pellet of casein micelles would come (very) close to the structure of the slab. Also, the scattering of a concentrated ultrafiltration retentate in the experiments of Pignon et al. [26] comes close to what we call a slab of casein micelle material. Also the concentrated samples prepared by Bouchoux [3] through osmotic dehydration resemble the casein slab material. There may be (minor) effects of the surface of the casein micelles, but these effects are very small and can be accounted for. The first step is to calculate the scattering profile from such a continuous phase consisting of casein, solvent and the CCPs. One then needs a model for the distribution the protein and of the CCP (in compliance with the three different models discussed in the previous section). As argued above, the caseins must be distributed quite homogeneously because secondary features in the SAXS scattering spectrum appear at $Q \approx 1\ nm^{-1}$ corresponding to a radius of 3 nm.

The second step is to correct for the fact that casein micelles have a finite size. To do this, we introduce a scissor function $\Theta(\mathbf{r})$, which has a value of 1 within a particle and is zero everywhere else

$$\Theta(\mathbf{r}) = \begin{cases} 1, & \text{inside the particle,} \\ 0, & \text{outside the particle,} \end{cases} \tag{11}$$

and express the scattering length density for the continuum plus a particle as

$$\rho(\mathbf{r}) = \rho_\infty(\mathbf{r}).\Theta(\mathbf{r}), \tag{12}$$

where $\rho_\infty(\mathbf{r})$ is the scattering length density profile of the infinite medium.

Here we make the only approximation in our approach to calculate the scattering profile. We assume that the internal structure of a casein micelle particle is independent of the position within the particle. In particular, our 'scissors' may cut through a few CCP particles, but this will not influence the result. This is very reasonable since the number of CCP particles is at least several hundred and depending on the model several thousand. After some mathematical calculations, which are described in more detail in Appendix A, we arrive at the following expression for the scattering intensity of a casein micelle.

$$I_{total}(Q) = |\bar{\rho}|^2 * PI_{cmpol}(Q) - \frac{4R^4}{V}\int_0^\infty I_\infty(Q')\frac{Q'}{Q}\{F[R(Q+Q')] - F[R(Q-Q')]\}dQ'. \tag{13}$$

Where the function $F(z)$ in the second term at the right hand side is given by:

$$F(z) = \frac{(\sin z - z\cos z)^2 + (z\sin z)^2}{4z^4} \tag{14}$$

The function $F(z)$ originates in the scissor function that cuts out the casein micelle. The variable Q' is an auxiliary wave vector parameter which is integrated out.

The casein micelle particle radius is given by R. The function $I_\infty(Q')$ represents the scattering profile of the "infinitely" large slab of material introduced above.

$$I_\infty(Q') = \Delta\rho^2_{CCP} PI_{CCP}(Q')S_{CCP}(Q') + \Delta\rho^2_{prot} PI_{prot}S_{prot}(Q') \tag{15}$$

The form factor function $PI_{CCP}(Q')$ is the scattering of the CCP and is adapted to the polydisperse nanocluster model, or the Angstrom cluster model. In addition, we assumed a lower protein density in a layer of 2 nm near the surface of the CCP due to protein adsorption. The form factor PI_{prot} function accounts for the fact that the protein will not be smeared out completely but that it will have small regions of increased density, particularly where the hydrophobic parts meet. Since the slab of material is homogeneous with respect to the distribution of the protein and the solvent the contrast $\Delta\rho_{CCP}$ is the difference between the SLD of the CCP and the solvent. Thus we assume a hierarchical structure. The smallest scale is the solvent, the next level is the protein few nm-scale and the final level is the distribution of the nanoclusters with a protein layer but on average 18.6 nm apart, dispersed in the protein matrix. We assume that the distribution of the different substructures is independent of each other. The correlation between the structural elements is accounted for by the structure factor $S(Q')$. The experimentally found correlation length in the scattering experiment is 18.6 nm. We assumed a liquid like structure in the distribution of the CCP and used the Percus-Yevick equation [39, 40] for the hard sphere fluid to model this distribution of the CCP. Then the first peak of the structure factor appears at approximately $0.35\ nm^{-1}$. By choosing the effective volume fraction the height of the peak is varied. We used 0.40 but found that a value for the effective packing can be varied between 0.30 and 0.55. We could have used other expressions for the structure factor, e.g., for adhesive spheres or repulsive spheres but that would introduce an extra parameter and results would not be different. A fractal packing would of course not suffice, since it has no typical correlation length. We preferred the simplest model with the least i.e. one adjustable parameter. One may wonder why the nanoclusters are separated on average by a distance of about 18.6 nm. We think that this is caused by the fact that the hydrophilic phosphate centers of the caseins bind to the CCP. As a result hydrophobic ´tails´ of the caseins stick out. These tails will entangle with other hydrophobic tails forming small hydrophobic and denser protein regions of about 2 nm in size. In Fig. 4 we present the functions from Eq. (15).

In case of the nanoclusters (nc), there are about 287 per (volume averaged) casein micelle and in case of the mini-clusters we would

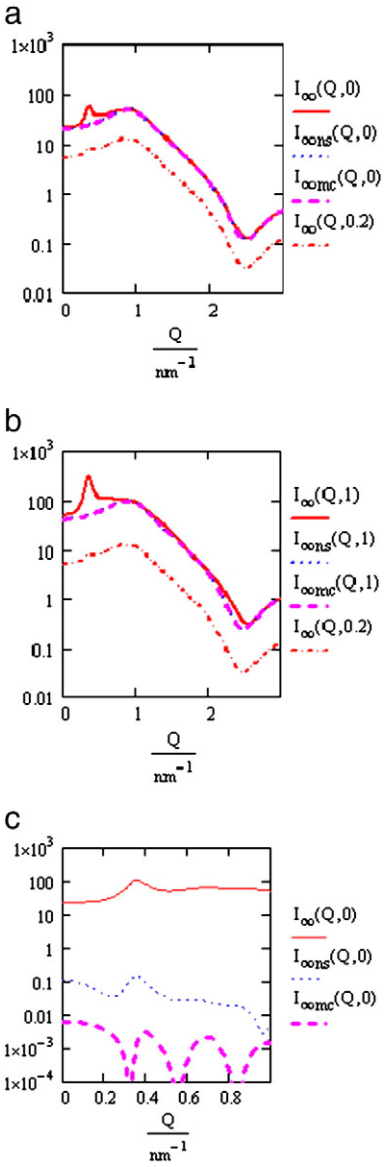

Fig. 4. a) SANS, Calculated $I_\infty(Q',\Phi=1)$ for the nanocluster (nc, full line) and the Angstrom shell (as, dashed)model both dashed and the Angstrom-cluster model (ac, dotted), Panel A casein micelles in H2O, Panel B Casein micelles in D2O, Panel C for SAXS.

have about 5 times more. Of course the volume of the Angstrom-clusters (ac) v_{sph} is than 5 times smaller. Averaging the position of the (mono-disperse) Angstrom-clusters over the surface of the sub-micelle leads to the same result as the Angstrom shell (as) model. The more so we realized from these calculations that subdividing the nanoclusters into 5 angstrom-clusters lowers their contribution to scattering by a factor factor of 5. In Fig. 4 we present the calculated scattering intensity $I_\infty(Q',\Phi=1)$of the nanoluster and the Angstrom shell model. $\Phi=1$ means that solvent is pure D_2O.

Fig. 4 indicates that maximum contribution to scattering is obtained from the NC in D_2O. All other conditions give a much lower intensity. If the correlation peak at $Q\approx 0.35\ nm^{-1}$ generates the shoulder in SANS spectra than it is to be expected that this shoulder is not visible in for instance SAXS spectra.

The functions shown in Fig. 4 must be convoluted with the function $F(z)$ as in Eq. (14). Only at small Q, there is a slight difference for the non-convoluted and convoluted scattering function. Of course there is a strong difference between the nanocluster and the Angstrom shell model. In both cases, we included the same structure factor $S(Q)$ which only modulates the data. So, we assumed the same packing fraction for the nanoclusters and the Angstrom shells. Of course for both models, the ordinate value must be identical for mono disperse particles and reflects molar mass. The CCP on the periphery of a 'sub-micelle' are 5-times smaller in volume than the nanoclusters if located at the 'center'. Also at this point it is relevant that in the ''classical" models where the CCP is located at the periphery of the sub-micelle, it is necessary that the CCP clusters are very small (1.4 nm) from total mass and geometrical considerations i.e. 10 'contacts' per sub-micelle. Fig. 4a shows two shoulders one at $Q=0.35\ nm^{-1}$and one at $Q=1\ nm^{-1}$. The first shoulder is not visible in SANS at the H_2O side and not in SAXS because of the low contrast. If we set $S(Q)=1$, then the secondary maximum disappears completely from all scattering functions. The form factor for a mono-disperse sphere $P(Q)$ (see Eq. (8)) and the polydisperse form factor $P_{cmpol}(Q)$ (see Eq. (9)) are shown in Fig. 5. Clearly all details are washed out.

Please note that the fluctuations in $P_{cmpol}(Q)$ are due to numerical calculations.

Also note that the minima in the form factor of the casein micelle particle are on a much smaller scale than the features in the CCP scattering. Also these minima would be completely washed out by instrumental smearing if not already by particle poly-dispersity. The total scattering than follows by appropriately summing the functions in Figs. 4 and 5 according to Eq. (13). All calculations were made in a MATHCAD 14 program including dimensions of the parameters. Intensities were correctly found as m^{-1}.

5. Materials and Methods

5.1. Milk samples

Over the years we used three different milk samples for our studies. Main results presented here were obtained on one particular sample which we will describe in detail. From an extensive dynamic light scattering investigation on milk samples from 18 different cows we found that the casein micelle size is constant for a given cow during milking, lactation and over the years. In addition polydispersity varies from $\beta=0.27$ to $\beta=040$. It seemed that β was a linear function of the radius as is expected for particle stabilized by a ˝surfactant˝ molecule. We used the milk of a one cow (cow68, Martha183) as this milk had relatively small casein micelles and a relatively low polydispersity. Serum protein free casein micelle dispersions of this milk sample were prepared by centrifugal removal of fat (2000 x g for 20 min at 5 °C), followed by pelleting the casein

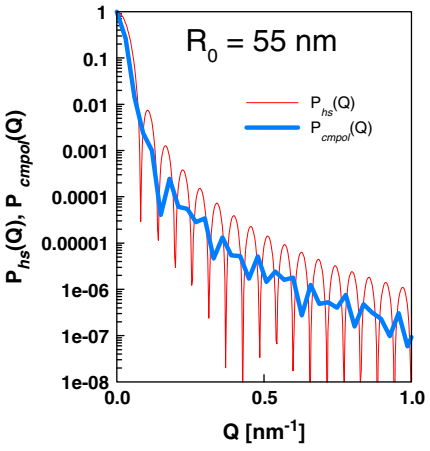

Fig. 5. Form factor, P(Q,) (Eq. (8)),of a mono-disperse homogeneous sphere and the form factor of a collection of poly-disperse homogeneous spheres.(Eq. (9)) $R_{10}=55$ nm, $\beta=0.27$, $R_{gyr}=90$ nm, $R_{hydr}(90^g)=80$ nm The small fluctuations are due to numerical inaccuracies.

micelles in the defatted milk by ultracentrifugation and resuspension, at a casein concentration of 2.5% (m/m) in the 10 kDa filtrate of the original milk, as described in detail by Huppertz et al. [43]. The casein micelle suspension were used for static and dynamic light scattering directly and were subsequently lyophilized and resuspended in mixtures of H_2O and D_2O for scattering measurements. Resuspended samples were also used for light scattering, which indicated that lyophilization and subsequent resuspension did not affect particle size.

The experiments with the cross linked casein micelles, called casein nanogels, were made on casein micelles isolated from reconstituted serum protein-free milk powder (NIZO food research, Ede, The Netherlands) using the procedure outlined above. The samples were subsequently subjected to enzymatic cross-linking using the enzyme transglutaminase (TGase) as described by Huppertz et al. [43].

The casein micelles used by Holt et al. [23] were prepared at the HANNAH research institute Ayr Scotland. Casein micelles from fresh skimmilk were pelleted by ultracentrifugation (25,000 g for 30 min at 20 °C) before resuspension in a buffer designed to be saturated with respect to CP. The composition and preparation of such buffers has been described previously [12] where they were used to dilute casein-calcium phosphate complexes, while preserving their integrity. The standard resuspension buffer had a free calcium ion concentration of 2 mM, ionic strength of 80 mM and pH of 6.7.

At this point we would like to make the following remark. Although different investigations used (slightly) different methods of preparation there is a broad agreement on the essential features of the scattering spectra both from SANS and SAXS. We therefore are confident that preparation had no essential influence on the results.

5.2. Scattering set ups

SANS measurements were made at the ILL (Grenoble, France) on the D22 spectrometer, at ISIS (Didcot, UK) on LOQ. The SANS data on milk from cow 68, Martha 183 and presented herewith were obtained at Oak Ridge National Laboratory on SANS CG2. SAXS measurements were made at the ESRF in Grenoble on ID2.

Static and dynamic light scattering were made on an ALV goniometer with four APD-detectors using a fast correlator of CORRELATOR.COM. and a 200 mW solid state VERDI laser Rayleigh ratio's were obtained by normalizing the time averaged intensity on the scattering of purified toluene. Data were taken at 16 different angles from 17 to 150 degrees. Samples were diluted 10 and 100 times with milk serum so as to avoid multiple scattering.

6. Results and discussion

In separate and extensive experiments we characterized the casein micelles used in the SANS experiments reported herewith. In addition we used data from literature. It was our aim to use independently determined parameters for the model calculations. In that way we may calculate/predict the scattering spectra and not fit the data to calculated spectra.

By doing so were able to test models put forward for the structure of casein micelles. Particle size, density and mass cannot be varied independently and data from different measurements must be self consistent.

6.1. Dimensions of the casein micelles

From our static and dynamic light scattering experiments we found that milk of individual cows has a low(er) polydispersity than pooled tank milk. Also we found that the casein micelle size of a cow is constant during milking, lactation and over the years. For this reason we selected the milk of one particular cow (Martha 183) for new SANS and SAXS experiments. We collected milk from this cow 68 (Martha 183) in three subsequent years.

In Fig. 6 we present the measured hydrodynamic radius. Assuming a ln-normal distribution, we simulated the intensity auto-correlation function from which we than calculated the apparent hydrodynamic radius.

The drawn line in Fig. 6 with $\beta = 0.27$ represents the data quite well. This line is obtained with a median particle radius of 55 nm and a polydispersity of $\beta = 0.27$. The data at the lowest Q-values are noisy most probably due to residual dust, fat or aggregates. The data for scattering angles larger than 45 degrees are constant in time (milkings over 3 years period) indicating that the variation at low angles derives from artifacts. Thus from DLS measurements we find $R_0 = 55$ nm with $\beta = 0.27$. Then the volume average radius is $R_v = 61$ nm the radius of gyration $R_g = 90$ nm and the DLS radius $R_{65} = 80$ nm. These values are consistently lower than what is found for pooled milk, which has a larger median and a higher polydispersity.

The number of CCP particles in a micelle is determined by the condition that the coordination length is 18.6 nm so as to lead to a correlation shoulder in the spectra at 0.35 nm^{-1}. In a liquid like or random structure of spheres the correlation length is virtually equal to twice the radius of the spheres. This means that in the sub-micelle models the ˝substructures˝ have a radius of 9.3 nm. Now the CCP is either at the periphery or at the center of the ˝substructures˝. In the nanocluster model, the sub-micelles do not exist and in that case the average distance between the center of the nanoclusters is 18.6 nm. Thus the number of ˝sub-micelles˝ or CCP clusters is equal to $(R_{vol}/9.3\ nm)^3 = (61.1/9.3)^3 = 285$ per casein micelle used here. Naturally, the number of sub-micelles or nanoclusters per micelle will depend on micelle size. Since the mass of CCP is 7% of the dry mass this determines the mass per CCP cluster as well and density is $Mass_{nc}/V_{nc}$. The number of NC fixed and their mass is fixed (7% of the total mass) than the only parameter left is density. If we presume that density is the density of hydroxyapetite (2.31 kg/L) than the median radius is 1.72 nm. Since Holt gave a larger value for his synthetic NC we assumed a lower density of the NC of 1 kg/L which is probably a lower value and which accounts for the fact that it is expected that the NC are amorphous and heterogeneous structures, based on the result of Neville [17]. In that situation the NC have a median radius of 2.27 nm, and a volume average radius of 2.5 nm and a radius of gyration of 3.7 nm. Respectively 1.72 nm and radius of gyration of 2.85 nm), Of course SLD must be adjusted accordingly. We will use these two extremes for the size of the NC in our

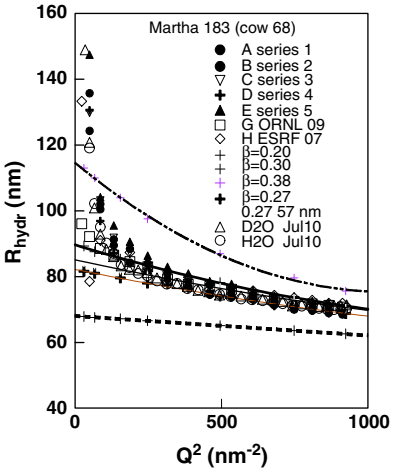

Fig. 6. Dynamic light scattering data for milk of cow 68 (Martha 183). Different milkings over a period of 3 years. The drawn lines represent different degrees of polydispersity.

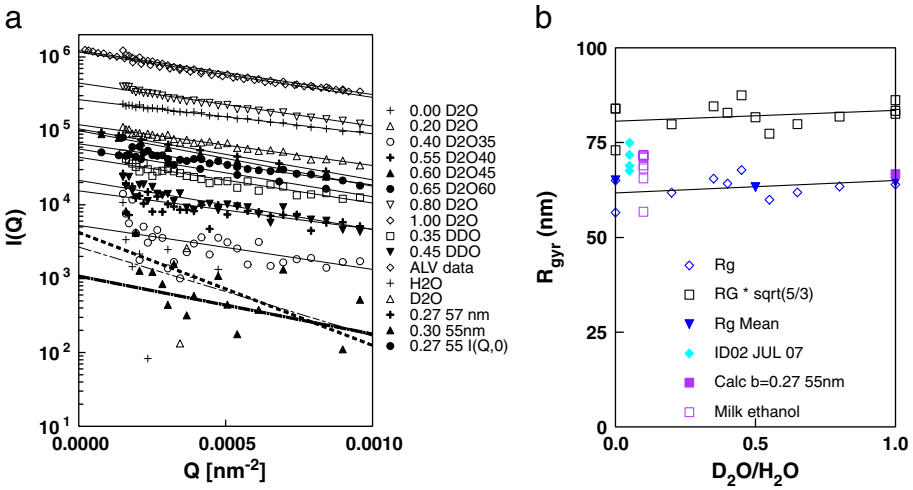

Fig. 7. a) Experimental Guinier plots at various D_2O/H_2O ratios. b) Calculated radius of gyration.

calculations. In the case of the 2.27 nm NC we assume that the clusters are amorphous and consist for 2/3 of exchangeable solvent.

6.2. SANS contrast variation of casein micelles

Based on previous experiences we prepared samples of various D2O/H2O content by volumetric mixing of samples in pure H_2O and D_2O. The samples were measured at the ORNL at two sample to detector distances of 18.5 m and 3 m. Spectra were merged using ORNL software. In Fig. 7, we present a Guinier plot of all the experimental data at the various contrasts.

We fitted (drawn lines in Fig. 7) the first 32 data points of all spectra in the Guinier plot. From this we obtained $I(Q=0, \Phi)$ and the Guinier slope which is equal to 1/3 R^2_{gyr}. In Fig. 8 we plot $I(Q=0, \Phi)/ I(Q=0, \Phi=0)$ which is equal to $\Delta\rho(\Phi)^2/\Delta\rho(0)^2$.

Fig. 8 shows that measured and calculated contrast are in good agreement. Contrast matchpoint is near $\Phi=0.41$. In Fig. 7b we plot the Guinier slope which is virtually independent of contrast. These are important results as they confirm that the used SLD are correct and more importantly that the distribution of matter in a casein micelle is homogeneous on the scale of a CM. It is known that D_2O has a (stabilizing) effect on the native structure of folded proteins [58] and promotes micellization of β-casein [62]. The poorer solvent quality of D2O might induce secondary structure, but these structures would be invisible near the protein matchpoint, i.e., near a D_2O volume fraction of ~0.41. Therefore and again the shoulder at 0.35 nm^{-1} must be due to the CCP.

What the influence of D_2O is on the structure of casein micelles is unknown. However here we find that the R_{gyr} does not change. We also found from DLS measurements (see Fig. 6) for three completely different casein micelle samples that the R_{hydr} is the same in H_2O and D_2O. The experimental results in Fig. 8 were obtained at the ORNL and the data of Holt et al. [23] at the ILL. Please note that these were two different samples prepared somewhat differently and probably somewhat different in concentration. As a whole both series are quite consistent and show the features at the respective values of the contrast.

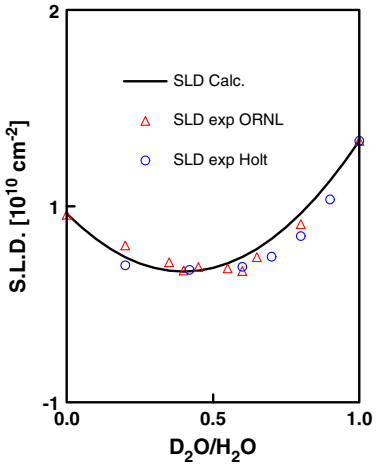

Fig. 8. Experimental contrast and calculated contrast as a function of fraction D_2O in the dispersion medium. Data collected by Holt at the ILL and this work at ORNL. Data normalized to scattering in H_2O.

6.3. Model calculations

In order to make the model calculations, we wrote a computer program in MathCad 14 that evaluated the pertinent equations numerically. We fixed the median size of the casein micelles to 55 nm and $\beta=0.27$. (since we used the milk of Martha 183) and these numbers were determined separately and independently in extensive DLS, SLS, viscosity and sedimentation experiments, to be published) From viscosity measurements it follows that voluminosity is 4.4 ml/g a value confirmed by Shukla [30] from SAXS measurements. From sedimentation velocity measurements we find the overall density of the casein micelles 1.078 kg/L whereas the density of the serum was found as 1.023 kg/L. Therefore the density of the protein is

$$\mathrm{dens}_{\mathrm{prot}} := \left(1.078\frac{\mathrm{kg}}{\mathrm{L}} - \frac{3.4}{4.4}\cdot 1.023\frac{\mathrm{kg}}{\mathrm{L}}\right)4.4$$

These data from experiment will be used further in our calculations. The volume averaged radius is $(4/(3\pi)\ V_{cm})^{1/3}=61.1$ nm. The number of casein micelles in undiluted milk is $N_{cm}=0.11/V_{cm}=1.14\ 10^{17}\ L^{-1}$. Another way of calculating the number of casein micelles is in milk containing 3% of dry casein protein is: $N_{cm}=0.03\ kg.L^{-1}\ /(V_{cm}.\ d_{prot}\ .1/4.4)=1.08\ 10^{17}\ L^{-1}$. So virtually the same as before. We used for density of the protein $d_{prot}=1.265\ kg\ L^{-1}$ which we found from sedimentation velocity measurements and which is the same as the result for a whole series of proteins [61]. The molar mass of the protein is 1.656 10^5 kg. and for a hydrated casein micelles 4.4. times larger or 0.62 10^6 kg. Shukla [30] found 2.2 10^6 kg from their SAXS data, which is about 3 times larger than our value. Shukla [30] used pooled milk where median CM size is about

70 nm and therefore molar mass will be about 2 times larger. With these numbers fixed the mass of the calcium phosphate is 7% of the protein.

The model calculations were made with Eq. (13) presented above. Comparing the calculated contributions of the CCP in the nanocluster model and the Angstrom shell model we see a clear difference in Fig. 4. If the CCP is distributed as nanocluster or as an Angstrom shell at the periphery of a sub-micelle as suggested in the traditional casein micelle models and as reproduced in Fig. 3 This is best understood from the Angstrom cluster model. Since in this model the CCP is distributed over 10 nm sized clusters intensity goes down by a factor of 5 at $Q=0$. And the more so since an Angstrom cluster or Angstrom shell model depresses scattering at $Q\approx 0.35\ nm^{-1}$ and therefore the shoulder will not appear. The difference between the cluster and shell model originates in the fact that in the shell model the scattering particle has essentially larger dimensions and therefore scattering decays faster. In the nanocluster model the CCP is located in a compact sphere whose mass must be identical to the mass of the shell.

From the calculations presented in Fig. 4 it is clear that the characteristic shoulder at $Q\approx 0.35\ nm^{-1}$ in the SANS spectra of casein micelles is only present in D_2O rich solutions. Therefore we have presented the full calculations for the nanocluster model together with the relevant experimental data. As indicated above, calculations were made for two combinations (1,72 nm radius 2.31 kg L^{-1} density) and (2.27 nm radius 1 kg L^{-1}) for the NC. It appeared that the two different combinations resulted in hardly any difference in the scattering spectra as illustrated in the SAXS spectrum. The Angstrom cluster and Angstrom shell model do not reproduce the characteristics of the experimental data.

The shoulder in SANS spectra at $Q\approx 0.35\ nm^{-1}$ is observed independently in various studies [21-24, 43] and originates from the coordination or correlation of the nanoclusters. It is the effect of the structure factor that generates the shoulder. We included the same structure factor in both models. The structure factor was calculated from a hard sphere fluid in the Percus-Yevick approximation. It appears that an effective volume fraction of 0.40 gives satisfactorily results and is a rather acceptable value. An upper limit would be a random close packing volume fraction of 0.63. However it is expected that the effective value will be smaller because of polydispersity, and, maybe even more so, because there is no clear repulsion responsible for the structure.

From our model calculations we found that the scattering contribution of the NC would be too small. In addition the shoulder in SAXS data at $Q\approx 1\ nm^{-1}$ could not be reproduced while the shoulder at $Q\approx 0.35\ nm^{-1}$ is absent. Based on a large number of trial calculations we suggest that the CCP nanoclusters are stabilized by a protein coat of caseins which together form a protein matrix in which the nanoclusters are distributed more or less evenly. The protein matrix shows nm scale density fluctuations as a result of the weak interactions (hydrophobic interactions, hydrogen bonding, ion bonding, weak electrostatic Van der Waals attraction and other factors (but not the strong calcium phosphate interaction)). From SANS measurements on both β and κ casein we know that the hydrophobic tails form dense regions [53]. In the vicinity of the NC the protein matrix is less dense since that is the hydrophilic part of the protein. Therefore we modeled the system of NC with a corona of halve the average protein density dispersed in a protein matrix with denser areas of 2 nm radius separated at 6 nm distance. So a casein micelle contains about 3^3 times more protein clusters than NC. We realize this is a somewhat abstracted model of the protein distribution but it appeared to give consistent results. Calculations at different D_2O/H_2O contrast, varying between 0-1 gives quite satisfactorily results. Note there is a considerable change in the shape of the spectra but also in the scattering level. All of this is predicted quite consistently. The fact that at high(er) scattering wave vectors the calculated scattering is above the experimental spectra could be due to incorrect solvent subtraction. Due to H/D exchange, the solvent subtraction is not completely defined which is less so a problem in pure H_2O and pure D_2O. It is noted that in Fig. 8 the experimental contrast for $0.6<\Phi<1$ is systematically somewhat below calculated contrast, which may indeed be due to over-subtraction of solvent. For the ISIS data presented below the experimental data go below calculated spectra even more. The reason being that these data were corrected for incoherent scattering by applying Porods law , i.e. assuming that scattering tails off as ∞Q^{-4} as part of the data reduction procedure. This is/was not allowed since Q-values are not small enough yet.

6.4. Casein nanogels; cross-linked casein micelles

Previously we prepared casein nanogels by cross linking the caseins internally using pooled milk. We showed that all the caseins are cross-linked after 24 h incubation with transglutaminase and found no inter-micellar cross-linking from the SLS and DLS results [43, 55, 56, 57]. On adding 0-6 M urea both the SANS (at ISIS) and the SLS from these micelles were measured, where the SLS data extend the SANS data to very small Q, see Fig. 10. A Guinier plot showed that the ordinate changed [43] which can be accounted for fully by the change in contrast but the Guinier slope was unchanged. This shows that the cross linked micelles do not shrink or swell in urea. Non cross linked micelles completely dissociate in 6 M urea.

It is noteworthy that the spectra of the cross-linked casein micelles hardly differ from the native (i.e. non-cross-linked) casein micelles. Maybe the spectrum is slightly above the native casein micelles which would suggest a small shrinkage which is however not noticeable in the DLS experiments. The fact that the experimental data fall off more steeply at higher Q is due to the correction for incoherent scattering using Porods law.

Especially in SANS, the contrast is lowered by the addition of urea. Fig. 10 shows that contrast diminishes to a level comparable to 60% D_2O. On adding urea the turbidity (in visible light) of the system is diminished somewhat but this can be accounted for completely by changes in light scattering contrast [43]. In Fig. 10 we present the measured and calculated spectra using the SLD of urea in D_2O. The calculations follow the features of the experiments quite nicely. These results therefore suggest that the nanogels stay intact on adding urea, but also that the cross-linking prevents a considerable swelling of the nanogels. Static light scattering data did not indicate an appreciable change in size either, R_{gyr} is constant. The hydrodynamic radius as a function of wave vector increases by ≈20 nm on completely cross linking the casein micelles. We therefore attribute the apparent increase in hydrodynamic radius in 6 M urea (and in serum) to the presence of “dangling” ends since the urea disrupts the weak interactions. Small parts or a few casein molecules may serve as a drag and diminish diffusivity. It was shown by Stenkamp and Berg [59] that at polymer coverage of a latex particle as low as 1% of maximum coverage increases the hydrodynamic radius by almost the contour length of the polymer in a good solvent. The contour length of a casein molecule can be estimated to be ≈20 nm. A few dangling ends would however contribute little, if any, to the scattering profile of the nanogels. Therefore the data suggest that the nanogels are rather “frozen in” structures of the native casein micelles which do not swell even in a good solvent. One would then

Fig. 9. Model calculations and experimental SANS results on casein micelles at various D_2O/H_2O fractions e.g. 0.8 D_2O indicates 80% v/v D_2O. Note that all calculations were made using the nano cluster model. The last panel represents SAXS data and calculations. Calculated curves are indicated with K and plotted as Δ. ORNL data +, Holt's data as o.

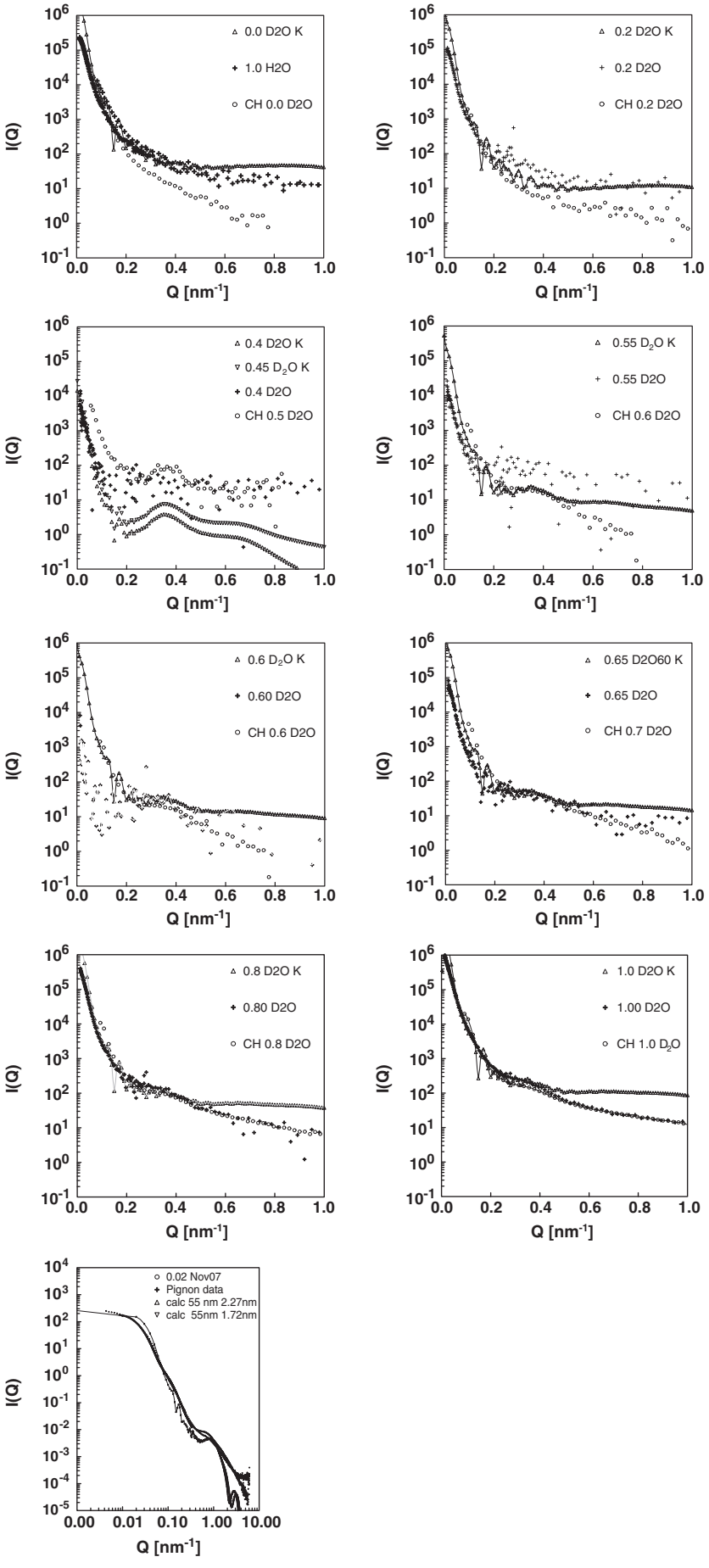
0.0 D2O K
1.0 H2O
CH 0.0 D2O
0.2 D2O K
0.2 D2O
CH 0.2 D2O
0.4 D2O K
0.45 D2O K
0.4 D2O
CH 0.5 D2O
0.55 D2O K
0.55 D2O
CH 0.6 D2O
0.6 D2O K
0.60 D2O
CH 0.6 D2O
0.65 D2O60 K
0.65 D2O
CH 0.7 D2O
0.8 D2O K
0.80 D2O
CH 0.8 D2O
1.0 D2O K
1.00 D2O
CH 1.0 D2O
0.02 Nov07
Pignon data
calc 55 nm 2.27nm
calc 55nm 1.72nm
I(Q)
Q [nm-1]

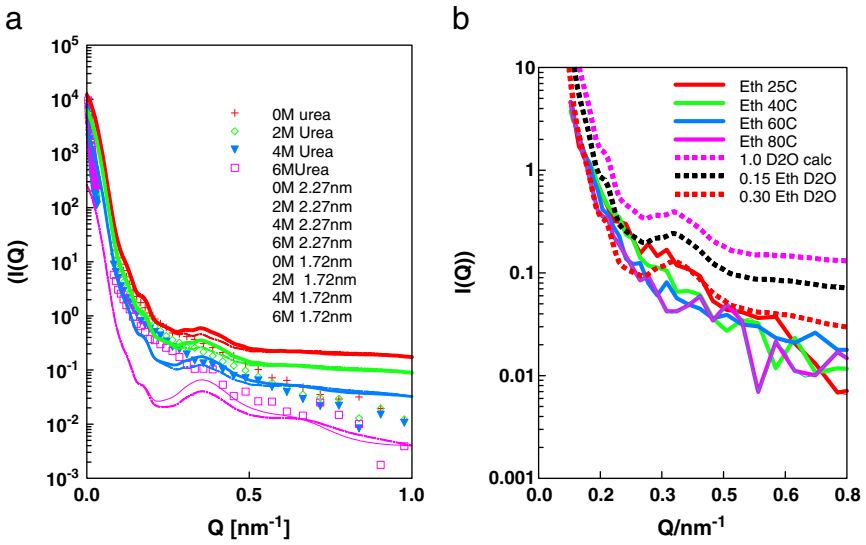

Fig. 10. a) Combined SLS (NIZO) and SANS (ISIS) spectra of cross linked casein micelles and nanogels with added urea b) Sans data on cross linked casein micelles in 1:3 ethanol/water . Symbols experimental data, drawn lines calculated.

expect that the steric stability of the nanogels is somewhat diminished due to the decreased conformational entropy of the surface moieties, which is indeed found [56].

Using the same casein nanogels as in the previous paragraph we measured SANS spectra at the ISIS of cross linked casein micelles in a 1:3 ethanol/D_2O mixture, see Fig. 10b. On adding 30% ethanol the casein micelle dispersion is marginally stable, but on heating to 65 °C, the milk becomes bluish and almost transparent, indicating that the casein micelles disintegrate in 30% ethanol at 65 °C [60, 61]. Fig. 10 shows the SANS spectra of cross linked casein micelles in 30% Ethanol/D_2O. If any, there is a slight tendency of the scattering intensity to dimish (very little). This may be attributed to the fact that we subtracted the solvent spectrum measured at 25 C which has a 2.5% higher density than solvent at 80 C. Also a very slight increase in size due to swelling would lower intensity at finite Q, but not the ordinate at Q = 0. Thus it seems that the casein nanogels remain almost unchanged or show a slight swelling in heated ethanol/water mixture. Although the data are somewhat noisy, the shoulder at $Q \approx 0.35\ nm^{-1}$ seems to diminish. This indicates that the protein matrix becomes more homogeneous. Indeed at 65 C the casein micelles dissociate indicating a ´good´ solvent condition. It was found [23] that the shoulder at $Q \approx 0.35\ nm^{-1}$ disappears on heating casein micelles in D_2O with 15% ethanol. In our model calculations the shoulder disappears on assuming a (more) homogeneous protein matrix. It is interesting to note that in the model calculation the shoulder at Q = 1 nm would increase in SAXS due to an increased contrast of the protein.

6.5. SAXS spectra

In Fig. 9i above we present SAXS spectra of two different (and different samples) investigations, which are virtually identical.

In Fig. 11a we show the influence of heating casein micelles dispersed in 1:3 ethanol water mixture. The data are in a smaller Q-range. The calculated line shows some oscillations which will be washed out in the experimental data due to polydispersity and instrumental smearing. In contrast to the experiments reported in Section 6.4, these micelles were not crosslinked. Fig. 11b shows the changes in the Guinier slope ($=-R^2_{gyr}/3$) and ordinate values i.e. ln(I(Q = 0)).

The Guinier slope remains constant or slightly increases while the ordinate value drops monotonously. This suggests that casein micelles disintegrate on heating in ethanol water but it is an all or nothing process. Suggesting that large(r) casein micelles are slightly more stable than the small micelles.

6.6. Overview of experimental and model parameters

In conclusion, we think that the nanocluster model gives consistent results. Also we think that the classical sub-micelle with the CCP located at the periphery of casein micelles is not consistent with observation and model calculation.

Parameters required for the model calculation were taken from independent investigations and the literature. These parameters are listed in Table 2 together with the experimental method. For evaluating data of pooled milk it will be necessary to increase R_{10} by 5 to 10 nm but also the polydispersity index β will increase from 0.27 to 0.35. Finally it must be remarked that the large dynamic range in intensity 4 – 6 decades makes it difficult to acquire low noise data over the whole Q-range of interest.

7. Conclusions

Native casein micelles in cow's milk were found to have a center radius $R_{10} = 61$ nm for pooled milk. The size polydispersity is 0.35 in a ln-normal distribution. DLS measurements would than give about 100 nm at 90 degrees scattering using a green laser. In the literature casein micelles are often called very polydisperse. However this is not consistent with the results presented herewith and with the expectation and experience that Mother Nature is not sloppy. Casein micelles of single cows are quite monodisperse and extremely constant in time.

In the literature, several models were proposed for the internal structure of the casein micelles. The oldest and most frequently cited model is the sub-micelle model based on the idea that caseins form micelles which are than glued together by colloidal calcium phosphate. A later model by Holt and based on experiments with casein nanoclusters views the casein micelle as a matrix of caseins in which the CCP nanoclusters are dispersed as very small (1.72 to 2.27 nm radius (median)) “cherry stones”. Attached to the surface of the nanoclusters are the centres of phosphorylation (3-5 nearby phosphate groups) of the caseins.

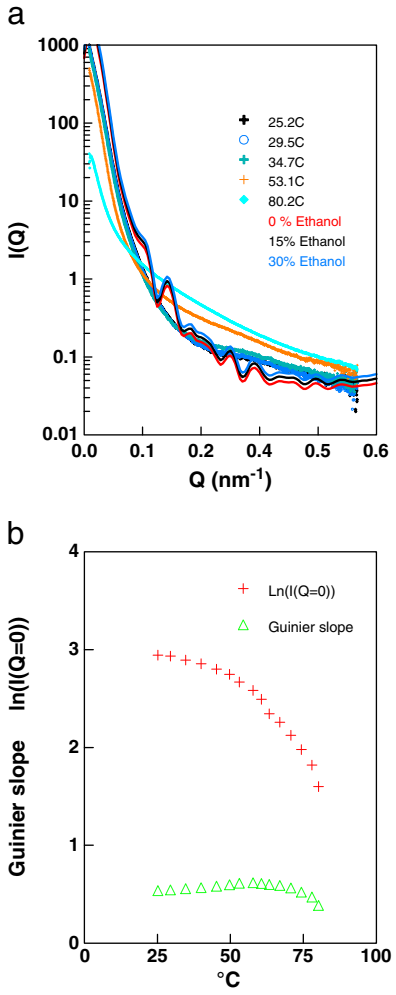

Fig. 11. Heated casein micelles in 1:3 ethanol/water mixtures.a) SAXS spectra at various temperatures. b) Ordinate and -Guinier slope as a function of temperature.

The tails of the caseins, much larger than the CCP clusters, associate to form a protein matrix with many small fluctuations in local protein density. The association of the tails is driven by a collection of *weak interactions*. We explicitly use *weak interactions* as a collective term as for hydrophobic, hydrogen bonding, ion bonding, weak electrostatic and Van der Waals attraction and other factors (but not the strong calcium phosphate interaction) leading to self association. The heterogeneity of the casein proteins could be taken as an indication for heterogeneity of the weak interactions. It is the cooperativety that leads to a stable casein micelle (as in Velcro). The interaction of only a pair of molecules, as suggested in the dual binding model, is thermodynamically unfavorable. Invariably κ-casein is thought to limit the process of self association leading to stabilization of the native casein micelle.

The nanocluster model and the sub-micelle model and variations thereon, e.g., the dual binding model, can be used to calculate the scattering in a SANS and SAXS experiment. Here we set up the necessary equations, and used in the calculations independently determined parameters taken from the literature. SLD values were calculated from the known protein and CCP composition of the casein micelles. Neutron contrast variation is an extremely valuable tool to determine the internal structure since SLD are known and therefore by changing contrast the scattering spectra must be predicted self consistently. We showed that the submicellar model was not consistent with experimental data. In retrospect there are additional arguments why the distribution of CCP in extremely small clusters of a few Angstroms (as in the dual binding model) is not very probable. The Angstrom sized clusters would be extremely instable and their contribution to the scattering is too low to notice, also in electron microscopy, wherefrom most of the support for sub-micellar structures was derived. The submicellar model generates a MINIMUM at $Q \approx 0.35$ nm^{-1} while there is a shoulder in the experimental data.

The nanocluster model appears to predict the spectra quite satisfactorily. Unfortunately experimental data suffer from uncertainties due to the large dynamic range in scattering (4-6 decades) but all principal features and certainly all trend/changes are predicted satisfactorily and more importantly self consistent with very limited adjustment of parameters.

Therefore it seems that the nanocluster model captures the main features of the casein micelle.

Further evidence was obtained by internally cross linking the native casein micelles with the help of an enzyme transglutaminase. The so formed nanogels have the same size as the starting material. The mean DLS-particle radius was 100 nm, due to the preparation of the whey protein-free milk, in which ultra- and micro-filtration was used.

On adding 6 M urea (some of the) weak interactions between the caseins in the nanogels were broken but that did not result in a change of size. Similarly sequestering the calcium did not change the particle radius (not shown). Scattering spectra could be predicted by taking into account the changed contrast. In DLS we observed a slight increase in Stokes radius on adding urea to the crosslinked micelles. This can be attributed to the presence of only a very few casein molecules extended in the good solvent serving as a drag anchor. On adding up to 30% ethanol the SAXS and SANS spectra change somewhat but that can be fully accounted for by changes in contrast. Heating casein micelles in 30% ethanol shows that the casein micelles swell slightly and than dissociate.

Table 2
Parameters used for the calculation of the SANS and SAXS spectra. Data were taken from literature and not adjusted or fitted except for the packing fraction and the size of the protein clusters, see discussion in text.

Parameter	symbol	Cow 68 (Pooled milk) [units]	Experimental
Casein micelle center rad.(ln-norm)	R_{10}	55 (60) [nm]	DLS
Polydispersity	β	0.27 (0.35) [-]	DLS
Volume averaged radius	R_3	61.1 (71.3) [nm]	Viscosity, DLS
Radius of gyration	R_{gyr}	90 (135) [nm]	SANS, SLS
DLS radius ($\lambda = 541, \Theta = 90$)	R_{hydr}	80 (100) [nm]	DLS
Voluminosity	-	4.4 [ml g^{-1}]	Viscosity
Mass density (hydrated)	-	1.078 [g ml^{-1}]	Analytical UC
Casein micelles per liter	N_{cm}	1.14 10^{17} [L^{-1}]	Calculated
Nanocluster	r_{nc}	1.72 to 2.27 [nm]	SANS/SAXS
Nanoclusters/ Casein micelle	N_{nc}	285 (372)	Calculated
Correlation length	ξ	9.3 [nm]	SANS
Packing fraction NC/prot. Clust.	-	0.4 / 0.2	estimated
Protein clusters	R_{prot}	2 nm	SAXS
Correlation length	ξ_{prot}	3 nm	SAXS

Acknowledgement

SANS experiments at Oak Ridge National Laboratory's Center for Structural Molecular Biology (CSMB) were supported by the Office of Biological and Environmental Research, using facilities supported by the U.S. Department of Energy, managed by UT-Battelle, LLC under contract no. DE-AC05-00OR22725. The authors also thank the European Synchrotron Radiation Facility (ESRF, Grenoble, France) for providing beamtime and Th. Narayanan for excellent support.

Dr Carl Holt (Glascow University) is thanked for the great many detailed discussions we had on the topic of casein micelles.We thank Henk de Kruif and his son Kees de Kruif (Woudenberg, The Netherlands) for allowing us to sample the cow's milk from their herd of Holstein Friesians. The assistance of Mary Smiddy (University College Cork / NIZO food research), Jan Klok (NIZO food research) and Dr. Jurgen Smeenk (NIZO food research) with the various experiments is greatly appreciated.

Appendix A. Scattering from composite particles

Since various conventions are found in the literature, we first explicitly specify our mathematical language. Scattering length density will be denoted as $\rho(\mathbf{r})$. Scattering amplitude $B(\mathbf{Q})$ is given by the 3-dimensional Fourier transform of $\rho(\mathbf{r})$.

$$B(\mathbf{Q}) = \int_{\mathbf{V}} \rho(\mathbf{r}).e^{i\mathbf{Q}.\mathbf{r}} d\mathbf{r} \tag{A1}$$

Here and after we omit unimportant pre-factors (a collection of constants and experimental parameters) for notation simplicity. For normalization convenience we assume that the integration is performed over a finite but very large sample volume V so that the sample size is much larger than any structural correlation length in the system. The $1/(2\pi)^3$ normalization factor will be included in the inverse Fourier transform.

$$\rho(\mathbf{r}) = \frac{1}{(2\pi)^3} \int_{-\infty}^{\infty} B(\mathbf{Q}).e^{-i\mathbf{Q}.\mathbf{r}} d\mathbf{Q}. \tag{A2}$$

Finally, the scattering intensity is given by the square modulus of the amplitude

$$I(\mathbf{Q}) = |B(\mathbf{Q})|^2. \tag{A3}$$

According to the correlation theorem, $I(\mathbf{Q})$ is the Fourier transform

$$I(\mathbf{Q}) = \int_{\mathbf{V}} \Gamma(\mathbf{r}) e^{i\mathbf{Q}.\mathbf{r}} d\mathbf{r} \tag{A4}$$

of the autocorrelation function,

$$\Gamma(\mathbf{r}) = \int_{\mathbf{V}} \rho(\mathbf{r}')\rho(\mathbf{r}'+\mathbf{r}) d\mathbf{r}'. \tag{A5}$$

Finally, $\Gamma(\mathbf{r})$ can be calculated from $I(\mathbf{Q})$ via the inverse Fourier transform

$$\Gamma(\mathbf{r}) = \frac{1}{(2\pi)^3} \int_{-\infty}^{+\infty} I(\mathbf{Q}).e^{-i\mathbf{Q}.\mathbf{r}} d\mathbf{Q}. \tag{A6}$$

As described in the main text, we assume that the particles are made of a medium with a known scattering profile $\tilde{I}_\infty(\mathbf{Q})$. The subscript ∞ reflects the fact that this is the Γ of an infinite medium. The use of a tilde above $\tilde{I}_\infty(\mathbf{Q})$ will be clarified further [Eq. (A12)]. Thus we consider a medium completely filled with casein micelles in such a way that no interstices are left. So we may say that $\tilde{I}_\infty(\mathbf{Q})$ is the profile of a bulk fused cheese curd matrix (but with the κ-casein still present). Using Eq. (B6), one can calculate the autocorrelation function $\Gamma_\infty(\mathbf{r})$ for this medium. Then we "cut out" the casein micelles from this slab with the scissor function $\Theta(\mathbf{r})$ given by Eq. (13). Since this procedure leads to $\rho(\mathbf{r}) = 0$ outside the particle, the scattering length density is defined relative to that in the solvent.

The assumption of the statistical independence of the $\rho(\mathbf{r})$ and $\Theta(\mathbf{r})$ functions leads for the autocorrelation function of the solvent with a particle to

$$\begin{aligned}\Gamma_{total}(\mathbf{r}) &= \int_{\mathbf{V}} \rho_\infty(\mathbf{r}')\rho_\infty(\mathbf{r}'+\mathbf{r})\,\Theta(\mathbf{r}')\Theta(\mathbf{r}'+\mathbf{r}) d\mathbf{r}' \\ &= \frac{1}{\mathbf{V}} \int_{\mathbf{V}} \rho_\infty(\mathbf{r}')\rho_\infty(\mathbf{r}'+\mathbf{r}) d\mathbf{r}' \int_{\mathbf{V}} \Theta(\mathbf{r}')\Theta(\mathbf{r}'+\mathbf{r}) d\mathbf{r}' \\ &= \frac{1}{\mathbf{V}} \Gamma_\infty(\mathbf{r})\Gamma_p(\mathbf{r}),\end{aligned} \tag{A7}$$

where $\Gamma_p(\mathbf{r})$ is the autocorrelation of particles with the 'scattering length density' $\Theta(\mathbf{r})$. The total scattering profile $I_{\text{total}}(\mathbf{Q})$ of the composite particles is given by the Fourier transform of the Γ_{total} [Eq. (A4)]. According to the convolution theorem the Fourier transform of a product of two functions is equal to the convolution of their Fourier transforms

$$I_{\text{total}}(\mathbf{Q}) = \frac{1}{(2\pi)^3 V} \int \tilde{I}_\infty(\mathbf{Q}')I_p(\mathbf{Q}-\mathbf{Q}')d\mathbf{Q}'. \tag{A8}$$

Usually, in scattering the absolute value of the scattering length density $\rho(\mathrm{r})$ is not important. Only the scattering *contrast* leads to scattering. Indeed, if one adds a constant value to $\rho(\mathbf{r})$ in Eq. (A2), the Fourier amplitudes will remain unchanged for any non-zero value of Q. It will only affect the amplitude of the δ-function at $Q=0$. For the composite particles we have defined the contrast relative to the solvent. It means that the average scattering length density inside the particle can be different from that of the solvent. This, in turn, will play a role since it will contribute to the contrast between the particle and the solvent. The δ-function contribution at $Q=0$ in the scattering function of the infinite medium will play a role in the scattering of the particles. Let us explicitly write down this term. Since the exact shape of the sample volume is not important, we can assume that it has the form of a cube and occupies the space between $-L/2$ and $L/2$ in all three Cartesian directions x, y, and z. For Q-values of the order of $2\pi/L$, *i.e.* on the scale much larger than the particle size, only the average value of the scattering contrast $\bar{\rho}$ relative to that in the solvent is of importance. By replacing $\rho(\mathbf{r})$ by $\bar{\rho}$ in Eq. (A1), we get

$$B_0(\mathbf{Q}) = \bar{\rho}L^3 \frac{\sin Q_x {}^{L}/_{2}}{Q_x {}^{L}/_{2}} \frac{\sin Q_y {}^{L}/_{2}}{Q_y {}^{L}/_{2}} \frac{\sin Q_z {}^{L}/_{2}}{Q_z {}^{L}/_{2}}. \tag{A9}$$

Here we added the subscript 0 to stress that this is the scattering amplitude $B(\mathbf{Q})$ in the vicinity of $Q=0$. Since L is much larger than any scale of interest, this is a very sharp peak, which can be approximated by a δ-function. Using the identity

$$\int_{-\infty}^{+\infty} \left(\frac{\sin x}{x}\right)^2 dx = \pi \tag{A10}$$

the intensity $I(\mathbf{Q}) = |B(\mathbf{Q})|^2$ at $\mathbf{Q}\to 0$ can be written as

$$I_0(\mathbf{Q}) = V|\bar{\rho}|^2(2\pi)^3\delta(\mathbf{Q}). \tag{A11}$$

The intensity $\tilde{I}_\infty(\mathbf{Q})$ entering Eq. (A8), should include this δ-function at $Q\to 0$. Thus,

$$\tilde{I}_\infty(\mathbf{Q}) = I_0(\mathbf{Q}) + I_\infty(\mathbf{Q}) = V|\bar{\rho}|^2(2\pi)^3\delta(\mathbf{Q}) + I_\infty(\mathbf{Q}), \tag{A12}$$

where $I_\infty(\mathbf{Q})$ is the conventional scattering profile, which does not have any δ-function at $\mathbf{Q}=0$. Finally, Eq. (A8) becomes

$$I_{total}(\mathbf{Q}) = |\bar{\rho}|^2 I_p(\mathbf{Q}) + \frac{1}{(2\pi)^3 V} \int I_\infty(\mathbf{Q}')I_p(\mathbf{Q}-\mathbf{Q}')d\mathbf{Q}'. \tag{A13}$$

This is an important general result, which expresses the scattering profile of the whole system through the two scattering profiles of the medium and the particle envelopes. It can be applied to particles of different forms and sizes and it is valid as long as the internal structure is uniform throughout the particles.

The three dimensional integral in Eq. (A13) can be reduced to one-dimensional for spherical particles with isotropic (on average) internal structure. In this case the intensities in Eq. (A13) are functions of the length of the wave vector only: $I_\infty(\mathbf{Q}) = I_\infty(Q)$ and $I_p(\mathbf{Q}) = I_p(Q)$. For a single sphere

$$I_p(Q,R) = \left(3v_{sph}\frac{QR\cos(QR) - \sin(QR)}{(QR)^3}\right)^2, \tag{A14}$$

where $v_{sph} = (4/3)\ \pi\ R^3$ is the particle volume. It is convenient to switch to polar coordinates in Eq. (A13). The integral then becomes

$$\int I_\infty(\mathbf{Q}')I_p(\mathbf{Q}-\mathbf{Q}')d\mathbf{Q}' = 2\pi\int_0^\infty\int_0^\pi I_\infty(\mathbf{Q}')I_p\left(\sqrt{Q^2+Q'^2-2QQ'\cos\theta}\right)Q'^2\sin\theta\ d\theta\ dQ' \tag{A15}$$

where θ is the angle between Q and Q'; and 2π originates from the integration over the azimuthal angle φ. Using the substitution $z = R(Q^2+Q'^2-2QQ'\cos\theta)^{1/2}$ one can transform the θ-integral into

$$\int_0^\pi I_p\left(\sqrt{Q^2+Q'^2-2QQ'\cos\theta}\right)\sin\theta d\theta = \frac{\left(3v_{sph}\right)^2}{R^2QQ'}\int_{R(Q-Q')}^{R(Q+Q')}\left(\frac{\sin z + z\cos z}{z^3}\right)^2 z dz, = \frac{\left(3v_{sph}\right)^2}{R^2QQ'}[F(R(Q+Q')) - F(R(Q-Q'))], \tag{A16}$$

where $F(z)$ is given by Eq. (16). Substitution of Eq. (A16) into (A13) yields Eq. (15) in the main text.

Let us consider the limit of large particles (much larger than any characteristic scale of their internal structure). This is a simple limiting test case, in which one can split the scattering into two different contributions, related to the particle shape and to their internal structure. At small Q (*i.e.* $QR \sim 1$) the scattering intensity is dominated by the first term in Eq. (15). The second term becomes important at large values of Q, (*i.e.* $QR >> 1$). Then $F(R(Q+Q'))$ in the integral can be neglected since the function $F(z)$ quickly decays at $z >> 1$. Moreover, $F(R(Q-Q'))$ can be approximated by a δ-function

$$F[R(Q-Q')] \approx \frac{2\pi}{3R}\delta(Q-Q'). \tag{A17}$$

After a straightforward integration in Eq. (15), one gets

$$I_{total}(Q) \approx |\bar{\rho}|^2\left[3v_{sph}\frac{(QR)\cos(QR) - \sin(QR)}{(QR)^3}\right]^2 + \frac{v_{sph}}{V}I_\infty(Q), \tag{A18}$$

which is an expected result for large particles.

References

[1] Fox PF. Milk proteins: general and historical aspects. In: Fox PF, McSweeney PLH, editors. Advanced Dairy Chemistry 1: Proteins. 3 rd edn. New York: Kluwer Academic / Plenum Publishers; 2003. p. 1–48.
[2] Biopolymers in Food Colloids: Thermodynamics and Molecular Interactions. The Netherlands: Maria Semenova and Eric Dickinson. Brill, Leiden; 2010.
[3] Antoine Bouchoux, Genevieve Gesan-Guiziou, Javier Perez, Bernard Cabane. How to Squeeze a Sponge: Casein Micelles under Osmotic Stress, a SAXS Study. Biophys J December 2010;99:3754–62.
[4] Swaisgood HE. Chemistry of the caseins. In: Fox PF, Sweeney PLH, editors. Advanced Dairy Chemistry—1, Proteins. 3 rd edition. New York (NY: Kluwer Academic/Plenum; 2003. p. 139–201. Part A.
[5] Schmidt DG. Association of caseins and casein micelle structure. In: Fox PF, editor. Developments in Dairy Chemistry. Barking, UK: Applied Science Publishers; 1982. p. 61–86.
[6] Rollema HS. In: Fox PF, editor. Casein Association and Micelle Formation. Advanced Dairy ChemistryBarking, Essex, UK: Elsevier Applied Science; 1992. p. 111–40.
[7] Holt C. Structure and stability of bovine casein micelles. Adv Protein Chem 1992;43:63–151.
[8] Holt C, Horne DS. The hairy casein micelle: Evolution of the concept and its implications for dairy processing. Neth Milk Dairy J 1996;50:1–27.
[9] International Dairy Journal Vol. 8(3) (1998) pp. 153-250. Special conference proceedings
[10] International Dairy Journal Vol. 9(3-6) (1999) pp. 161-420), Special conference proceedings
[11] De Kruif CG. Non-food applications of caseins. In: Aalbersberg WY, Hamer RJ, Jasperse P, de Jongh HHJ, de Kruif CG, Walstra P, de Wolf FA, editors. Progress in Biotechnology. Industrial Proteins in PerspectiveAmsterdam: Elsevier Science B.V; 2003. p. 259–63. 269.
[12] De Kruif CG, Holt C. Casein micelle structure, functions and interactions. In: Fox PF, McSweeney PLH, editors. Advanced Dairy Chemistry. Proteins, 3 rd ednNew York: Kluwer Academic/Plenum Publishers; 2003. p. 233–76.
[13] Fox PF, McSweeney PLH, editors. Advanced Dairy Chemistry. Proteins, 3 rd edNew York: Kluwer Academic/Plenum Publishers; 2003.
[14] Horne David S. Casein structure, self-assembly and gelation. Curr Opin Colloid Interface Sci 2002;7:456–61.
[15] Horne David S. Casein micelle structure: Models and muddles. Curr Opin Colloid Interface Sci 2006;11:148–53.
[16] Farrell Jr HM, Malin EL, Brown EM, Qi PX. Casein micelle structure: What can be learned from milk synthesis and structural biology? Curr Opin Colloid Interface Sci 2006;11:135–47.
[17] Neville Margaret C. Calcium Secretion into Milk. J Mammary Gland Biol Neoplasia April 2005;10 No. 2, April 2005 (C_ 2005).
[18] Edward Smyth, Roger A Clegg and Carl Holt A biological perspective on the structure and function of caseins and casein micelles International Journal of Dairy Technology Vol 57, No 2/3 May/August 2004
[19] Fox PF, Brodkorb A. The Casein Micelle: Historical Aspects, Current Concepts and Significance. Int Dairy J 2008;18:677–84.
[20] Ran Gao. Ion speciation in milk-like systems. Thesis, Wageningen University, 2010 SANS
[21] Stothart PH, Cebula DJ. Small-angle neutron scattering study of bovine casein micelles and sub-micelles. J Mol Biol 1982;160:391–5.
[22] Stothart PH. Subunit structure of casein micelles from small-angle neutron scattering. J Mol Biol 1989;208:635–8.
[23] Holt C, de Kruif CG, Tuinier R, M PA. Timmins Substructure of bovine casein micelles by small-angle X-ray and neutron scattering. Colloids Surf A: Physicochem Eng Aspects 2003;213:275–84.
[24] Hansen S, Bauer R, Lomholt SB, Bruun Qvist K, Pedersen JS, Mortensen K. Structure of casein micelles studied by small-angle neutron scattering. Eur Biophys J 1996;24 143-14.
[25] Pessen H, Kumosmski TF. H M Farrell Small-angle Xray scattering investigation of the micellar and submicellar forms of bovine casein. J Dairy Res 1989;56:443–51.
[26] Pignon F, Belina G, Narayanan T, Paubel X, Magnin A. G. Gésan-Guiziou Structure and rheological behavior of casein micelle suspensions during ultrafiltration process. J Chem Phys 2004;121:8138–46.
[27] Stéphane Marchin, Frédéric Pignon, Joëlle Léonil. Effects of the environmental factors on the casein micelle structure studied by cryo transmission electron microscopy and small-angle x-ray scattering/ultrasmall-angle x-ray scattering. J Chem Phys 2007;126:045101.
[28] Pitkowski A, Nicolai T, Durand D. Biomacromolecules 2008;9:369.
[29] Gebhardt R, Burghammer M, Riekel C, Roth SV, Muller-Buschbaum P. Macromol Biosci 2008;8:347.
[30] Anuj Shukla, Theyencheri Narayanan, Drazen Zanchib. Structure of casein micelles and their complexation with tannins. Soft Matter 2009;5:2884–8.
[31] Beaucage G. Approximations Leading to a Unified Exponential/Power-Law Approach to Small-Angle Scattering. J Appl Cryst 1995;28:717–28.
[32] Jacrot B. The study of biological structures by neutron scattering from solution. Rep Prog Phys 1976:911–53.
[33] Hayter JB. In: Degiorgio V, Corti M, editors. Ph\sics of amphiphües-micelles vesicles and microemulsions. Amsterdam: North Holland; 1985.
[34] Ibel K. J Appl Crytstallogr 1976;9:296.
[35] [a] Holt C, Timmins PA, Errington N, Leaver J. A core-shell model of calcium phosphate nanoclusters derived from sedimentation equilibrium and small angle X-ray and neutron scattering measurements. Eur J Biochem 1998;252: 73–8.
[b] Holt C, Little EM. An equilibrium thermodynamic model of the sequestration of calcium phosphate by casein phosphopeptides. Eur Biophys J 1998;33: 435–47.
[36] Jeurnink Theo JM, de Kruif Kees G. Printed in Clreat Britain Changes in milk on heating: viscosity measurement. J Dairy Res 1993;60:139–50.
[37] Morris*† GA, Foster ‡ J, Harding † SE. Further Observations on the Size, Shape, and Hydration of Casein Micelles from Novel Analytical Ultracentrifuge and Capillary Viscometry Approaches. Biomacromolecules 2000;1:764–7.
[38] de Kruif CG. Supra-aggregates of casein micelles as a prelude to coagulation. J Dairy Sci 1998;81:3019–28.
[39] Hansen JP, McDonald IR. Theory of Simple Liquids. New York: Academie Press; 1976.

[40] McQuarrie DA. Statistical Mechanics. New York: Harper & Row; 1976.
[41] McMahon DJ, Oommen BS. Structure of the casein micelle. J Dairy Sci 2008;91: 1709–21.
[42] Dalgleish Douglas G. On the structural models of bovine casein micelles—review and possible improvements. Soft Matter 2011;7:2265–72 2265.
[43] Huppertz Thom, Smiddy Mary A, de Kruif Cornelis G. Biocompatible Micro-Gel Particles from Cross-Linked Casein Micelles. Biomacromolecules 2007;8:1300–5.
[44] Waugh DF. The interaction of αs, β- and κ-caseins in micelle formation. Faraday Society Discuss 1958;25:186–92.
[45] Schmidt DG. Association of caseins and casein micelle structure. In: Fox PF, editor. Developments in Dairy Chemistry. Barking, UK: Applied Science Publishers; 1982. p. 61–86.
[46] Walstra Pieter. On the Stability of Casein Micelles. J Dairy Sci 1990;73 1%5-1979.
[47] Walstra P. Casein sub-micelles: do they exist? Int Dairy J 1999;9:189–92.
[48] David S. Horne Casein micelles as hard spheres: limitations of the model in acidified gel formation. Colloids Surf A: Physicochem Eng Aspects 2003;213 255_/263.
[49] Wouterse A, Philipse AP. Geometrical cluster ensemble analysis of random sphere packings. J Chem Phys 2006;125 194709.
[50] Yearbook / Hannah Research Institute, Ayr, University of Glasgow. 1999
[51] Stieger M, Richtering W, Pedersen JS, Lindner P. Small-angle neutron scattering study of structural changes in temperature sensitive microgel colloids. J Chem Phys 2004;120:6197–206.
[52] de Kruif CG, Grinberg VY. Micellisation of b-casein. Colloids Surf A: Physicochem Eng Aspects 2002;210:183–90.
[53] de Kruif CG, Tuinier R, Holt C, Timmins PA, Rollema HS. Physicochemical Study of *K*- and b-Casein Dispersions and the Effect of Cross-Linking by Transglutaminase. Langmuir 2002;18:4885–91.
[54] Mikheeva LM, Grinberg NV, Grinberg VYa, Khokhlov AR, de Kruif CG. Thermodynamics of micellization of bovine ß-casein studied by high-sensitivity differential scanning calorimetry. Langmuir 2003;19:2913–21.
[55] Smiddy MA, Martin J-EGH, Kelly AL, de Kruif CG, Huppertz T. Stability of Casein Micelles Cross-Linked by Transglutaminase. J Dairy Sci 2006;89(6):1–9.
[56] Huppertz T, de Kruif CG. Ethanol stability of casein micelles cross-linked by transglutaminase. Int Dairy J 2007;17:436–41.
[57] Huppertz T, de Kruif CG. Rennet-induced coagulation of enzymatically cross-linked casein micelles. Int Dairy J 2007;17:442–7.
[58] Marleen Verheul, Roefs Sebastianus PFM, de Kruif Kees G. Aggregation of L-lactoglobulin and in£uence of D2O. FEBS Lett 1998;421 273^276.
[59] Stenkamp Victoria S, Berg* John C. The Role of Long Tails in Steric Stabilization and Hydrodynamic Layer Thickness. Langmuir 1997;13:3827–32.
[60] O'Connell JE, Kelly AL, Fox PF, de Kruif CG. Mechanism for the Ethanol-Dependent Heat-Induced Dissociation of Casein Micelles. J Agric Food Chem 2001;49(9): 4424–8.
[61] O'Connell JE, Kelly AL, Auty MAE, Fox PF, de Kruif CG. Ethanol-Dependent Heat-Induced Dissociation of Casein Micelles. J Agric Food Chem 2001;49(9):4420–3.
[62] Evans MTA, Phillips MC. The Conformation and Aggregation of Bovine α-CaseinA. II. Thermodynamics of Thermal Association and the Effects of Changes in Polar and Apolar Interactions on Micellization. Biopolymers 1979;18:1123–40.